

Biosynthesis of 8-O-Methylated Benzoxazinoid Defense Compounds in Maize

Vinzenz Handrick,^{a,1} Christelle A.M. Robert,^{b,1} Kevin R. Ahern,^c Shaoqun Zhou,^c Ricardo A.R. Machado,^b Daniel Maag,^d Gaetan Glauser,^d Felix E. Fernandez-Penny,^c Jima N. Chandran,^a Eli Rodgers-Melnik,^e Bernd Schneider,^a Edward S. Buckler,^e Wilhelm Boland,^a Jonathan Gershenzon,^a Georg Jander,^{c,2} Matthias Erb,^{b,2} and Tobias G. Köllner^{a,2,3}

^a Max Planck Institute for Chemical Ecology, 07745 Jena, Germany

^b Institute of Plant Sciences, University of Bern, 3013 Bern, Switzerland

^c Boyce Thompson Institute for Plant Research, Ithaca, New York 14853

^d Institute of Biology, University of Neuchâtel, 2009 Neuchâtel, Switzerland

^e Institute for Genomic Diversity, Cornell University, Ithaca, New York 14853

ORCID IDs: 0000-0002-8680-0687 (K.R.A.); 0000-0002-3643-7875 (S.Z.); 0000-0002-5961-1506 (D.M.); 0000-0003-4788-1565 (B.S.); 0000-0002-3100-371X (E.B.); 0000-0001-6784-2534 (W.B.); 0000-0002-1812-1551 (J.G.); 0000-0002-9675-934X (G.J.); 0000-0002-7037-904X (T.G.K.)

Benzoxazinoids are important defense compounds in grasses. Here, we investigated the biosynthesis and biological roles of the 8-O-methylated benzoxazinoids, DIM₂BOA-Glc and HDM₂BOA-Glc. Using quantitative trait locus mapping and heterologous expression, we identified a 2-oxoglutarate-dependent dioxygenase (BX13) that catalyzes the conversion of DIMBOA-Glc into a new benzoxazinoid intermediate (TRIMBOA-Glc) by an uncommon reaction involving a hydroxylation and a likely ortho-rearrangement of a methoxy group. TRIMBOA-Glc is then converted to DIM₂BOA-Glc by a previously described O-methyltransferase BX7. Furthermore, we identified an O-methyltransferase (BX14) that converts DIM₂BOA-Glc to HDM₂BOA-Glc. The role of these enzymes in vivo was demonstrated by characterizing recombinant inbred lines, including Oh43, which has a point mutation in the start codon of *Bx13* and lacks both DIM₂BOA-Glc and HDM₂BOA-Glc, and I14H, which has an inactive *Bx14* allele and lacks HDM₂BOA-Glc in leaves. Experiments with near-isogenic maize lines derived from crosses between B73 and Oh43 revealed that the absence of DIM₂BOA-Glc and HDM₂BOA-Glc does not alter the constitutive accumulation or deglycosylation of other benzoxazinoids. The growth of various chewing herbivores was not significantly affected by the absence of BX13-dependent metabolites, while aphid performance increased, suggesting that DIM₂BOA-Glc and/or HDM₂BOA-Glc provide specific protection against phloem feeding insects.

INTRODUCTION

To protect themselves from herbivores, plants synthesize diverse arrays of toxic metabolites. Benzoxazinoids are among the most important plant defense compounds in many grasses, including wheat (*Triticum aestivum*) and maize (*Zea mays*; Niemeyer, 2009). They are predominantly stored as glucosides in the vacuoles and are enzymatically hydrolyzed into the respective aglucones and sugars upon tissue injury (reviewed in Niemeyer, 2009). Subsequent nonenzymatic breakdown of the unstable aglucones leads to the formation of highly reactive metabolites that are toxic to a wide range of chewing and phloem-feeding insect herbivores and plant pathogens (Niemeyer, 2009). However, certain herbivores can circumvent benzoxazinoid toxicity by reglucosylating the aglucones (Glauser et al., 2011; Wouters et al., 2014) and their breakdown products (Maag et al., 2014). Specialized maize feeders like the

western maize rootworm (*Diabrotica virgifera virgifera*) and the fall armyworm (*Spodoptera frugiperda*) even use benzoxazinoids as foraging cues (Köhler et al., 2015; Robert et al., 2012).

The core biosynthetic pathway of the major maize benzoxazinoid 2-(2,4-dihydroxy-7-methoxy-1,4-benzoxazin-3-one)-β-D-glucopyranose (DIMBOA-Glc) has been extensively studied (Gierl and Frey, 2001; Jonczyk et al., 2008; reviewed in Frey et al., 2009). The biosynthesis starts in the plastids with the conversion of the shikimate pathway-derived indole-3-glycerol phosphate into indole, catalyzed by the indole-3-glycerol phosphate lyase benzoxazinoneless 1 (BX1). A subsequent stepwise introduction of four oxygen atoms by the P450 monooxygenases BX2, BX3, BX4, and BX5 leads to the formation of 2,4-dihydroxy-1,4-benzoxazin-3-one (DIBOA), the core structure of the benzoxazinoids. DIBOA acts as substrate for the UDP-glucosyltransferases BX8 and BX9, which transform the toxic compound into the stable glucoside (Glc) DIBOA-Glc (von Rad et al., 2001). A hydroxylation of DIBOA-Glc at C-7, catalyzed by the 2-oxoglutarate-dependent dioxygenase (2ODD) BX6, and a subsequent methylation of the introduced hydroxyl group, catalyzed by the O-methyltransferase BX7, lead to the production of DIMBOA-Glc in the cytosol (Jonczyk et al., 2008).

DIMBOA-Glc is the most abundant benzoxazinoid in young and undamaged leaves of many maize lines, reaching levels of up to

¹ These authors contributed equally to this work.

² These authors contributed equally to this work.

³ Address correspondence to koellner@ice.mpg.de.

The author responsible for distribution of materials integral to the findings presented in this article in accordance with the policy described in the Instructions for Authors (www.plantcell.org) is: Tobias G. Köllner (koellner@ice.mpg.de).

www.plantcell.org/cgi/doi/10.1105/tpc.16.00065

3 mg g⁻¹ fresh weight (Meihls et al., 2013). However, upon insect herbivory or fungal infestation, its derivative 2-(2-hydroxy-4,7-dimethoxy-1,4-benzoxazin-3-one)-β-D-glucopyranose (HDMBOA-Glc) accumulates and becomes the dominant benzoxazinoid (Oikawa et al., 2004; Glauser et al., 2011; Dafoe et al., 2011; Marti et al., 2013). Three homologous O-methyltransferases (BX10, BX11, and BX12; formerly designated BX10a, BX10b, and BX10c, respectively) convert DIMBOA-Glc into HDMBOA-Glc by S-adenosyl-L-methionine-dependent methylation of the hydroxamic group of DIMBOA-Glc (Meihls et al., 2013). After tissue maceration caused, for example, by chewing herbivores, DIMBOA-Glc and HDMBOA-Glc are hydrolyzed by endogenous β-glucosidases, resulting in the liberation of 2,4-dihydroxy-7-methoxy-1,4-benzoxazin-3-one (DIMBOA) and 2-hydroxy-4,7-dimethoxy-1,4-benzoxazin-3-one (HDMBOA), respectively (Babcock and Esen, 1994; Czjzek et al., 2000). Although both aglucones are unstable, nonenzymatic breakdown is faster for HDMBOA than for DIMBOA, and HDMBOA has been associated with increased resistance against leaf-chewing herbivores (Oikawa et al., 2004; Maresh et al., 2006; Glauser et al., 2011; Meihls et al., 2013). On the other hand, the decline in DIMBOA-Glc as a result of increased HDMBOA-Glc production has been shown to be associated with a reduction in callose deposition, which increases the plant's susceptibility to phloem feeding aphids (Ahmad et al., 2011; Meihls et al., 2013; Tzin et al., 2015).

Besides DIMBOA-Glc and HDMBOA-Glc, many maize lines produce significant amounts of other benzoxazinoid derivatives such as the 8-O-methylated compounds, 2-(2,4-dihydroxy-7,8-dimethoxy-1,4-benzoxazin-3-one)-β-D-glucopyranose (DIM₂BOA-Glc) and 2-(2-hydroxy-4,7,8-trimethoxy-1,4-benzoxazin-3-one)-β-D-glucopyranose (HDM₂BOA-Glc) (Cambier et al., 1999; Glauser et al., 2011). DIM₂BOA-Glc is most likely formed through the addition of a methoxy group to DIMBOA-Glc. HDM₂BOA-Glc, on the other hand, is likely derived from DIM₂BOA-Glc by methylation of the hydroxamic group and is also induced after herbivory (Glauser et al., 2011). In contrast to the other major benzoxazinoids, the biosynthesis and biological relevance of DIM₂BOA-Glc and HDM₂BOA-Glc are unknown.

To elucidate the biosynthesis of DIM₂BOA-Glc and HDM₂BOA-Glc, we took advantage of the sequenced genome of the maize inbred line B73 (Schnable et al., 2009), the availability of high-resolution physical and genetic maps (Wei et al., 2009; Zhou et al., 2009; Ganai et al., 2011), and the nested association mapping (NAM) population generated from 25 diverse maize inbred lines (Flint-Garcia et al., 2005; Yu et al., 2008; McMullen et al., 2009). Using quantitative trait locus (QTL) mapping combined with heterologous expression, we were able to identify enzymes involved in DIM₂BOA-Glc and HDM₂BOA-Glc formation. To understand the importance of the identified enzymes in benzoxazinoid biosynthesis, we analyzed the genetic basis of natural variation in constitutive and herbivore-induced DIM₂BOA-Glc and HDM₂BOA-Glc levels. Finally, the generation of near-isogenic maize lines that differ in their capacity to produce DIM₂BOA-Glc and HDM₂BOA-Glc allowed us to study the importance of these compounds for the interaction between maize and different herbivores. Our experiments show that DIM₂BOA-Glc and HDM₂BOA-Glc are produced through an unexpected intermediate and specifically increase maize resistance to aphids.

RESULTS

Natural Variation in Constitutive and Induced DIM₂BOA-Glc and HDM₂BOA-Glc

To identify genes responsible for the formation of DIM₂BOA-Glc and HDM₂BOA-Glc in maize, we first profiled the abundance of these compounds in the leaves and roots of different NAM parental maize lines. In the leaves, DIM₂BOA-Glc levels varied substantially, ranging from 17.6 ± 7.2 μg g⁻¹ fresh weight (FW) in the inbred line CML277 to 596.6 ± 174.1 μg/g FW in the inbred line P39 (Figure 1A). This pattern is consistent with earlier findings (Meihls et al., 2013). In the roots, concentrations varied between 42.4 ± 16.3 μg g⁻¹ FW in CML322 and 1021.8 ± 131.8 μg g⁻¹ FW in Mo18W. One inbred line, Oh43, produced no detectable amounts of DIM₂BOA-Glc in either leaves or roots. The constitutive concentrations of HDM₂BOA-Glc were lower than those of DIM₂BOA-Glc, with the highest concentrations being found in the leaves of M162W (34.7 ± 11.1 μg g⁻¹ FW) and the roots of CML277 (339.4 ± 49.1 μg g⁻¹ FW). Again, Oh43 contained no detectable amounts of HDM₂BOA-Glc in either of the tissues (Figure 1A). Several other lines produced no detectable amounts of HDM₂BOA-Glc. Apart from their consistent absence in Oh43, no significant correlations between leaf and root DIM₂BOA-Glc and HDM₂BOA-Glc levels were found across the different parental lines (Pearson product moment correlations, P > 0.05).

HDM₂BOA-Glc is known to be induced by biotic stresses such as pathogen infestation and insect feeding (Oikawa et al., 2004; Ahmad et al., 2011; Marti et al., 2013). Preliminary screens indicated that different NAM parental lines also differ in their inducibility (Supplemental Tables 1 and 2). We therefore profiled herbivore-induced changes in two NAM lines, B73 and P39, in detail. Leaves were wounded on one side of the midrib and treated with regurgitant of the generalist beet armyworm (*Spodoptera exigua*) to mimic herbivory (Erb et al., 2009). In both lines, DIM₂BOA-Glc concentrations did not significantly change upon this mock herbivory treatment. However, we observed a significant local accumulation of HDM₂BOA-Glc after application of insect regurgitant, which was more than 40-fold greater in P39 than in B73 (Figure 1B; Student's *t* test, P < 0.05). No changes in DIM₂BOA-Glc or HDM₂BOA-Glc were observed on the other side of the midrib of the induced leaves (Supplemental Figure 1).

Mapping of Constitutive and Induced DIM₂BOA-Glc and HDM₂BOA-Glc Production Revealed Three QTLs on Chromosomes 2 and 4

Based on our initial screening, we performed several QTL mapping experiments using recombinant inbred lines derived from crosses between B73 and the other NAM lines. Due to the significant differences between constitutive DIM₂BOA-Glc and HDM₂BOA-Glc content in leaves of the inbred lines P39 and B73 (Figure 1A; DIM₂BOA-Glc, *n* ≥ 4, P < 0.05; HDM₂BOA-Glc, *n* ≥ 4, P < 0.05), we first mapped constitutive production of both compounds in the recombinant inbred population B73 × P39. Mapping of DIM₂BOA-Glc revealed three QTLs, *Bb1*, *Bb2*, and *Bb3* (*benzoxazinoid biosynthesis 1 to 3*), located on chromosomes 2 and 4 (bins 2.05,

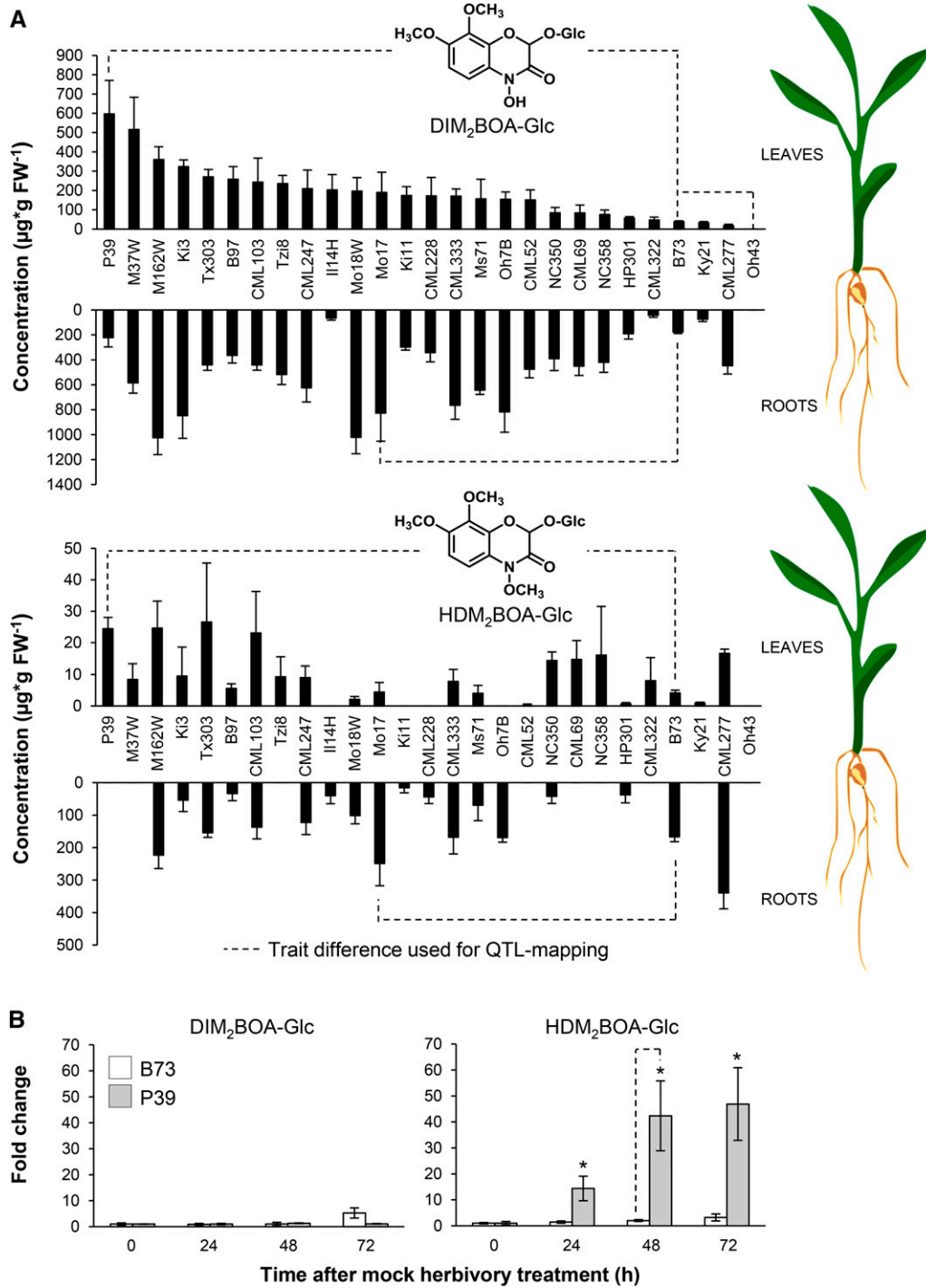


Figure 1. Benzoxazinoid Abundance in Leaves and Roots of the NAM Parental Lines.

(A) DIM₂BOA-Glc (top) and HDM₂BOA-Glc (bottom) concentrations in the leaves and roots of the NAM parental lines. Lines are sorted by average leaf concentrations. DIM₂BOA-Glc was not detectable in line Oh43. Means and standard errors (±se) are shown (n = 3 to 6).

(B) Induction of DIM₂BOA-Glc and HDM₂BOA-Glc in the leaves of the lines B73 and P39 at different time points. Herbivory was mimicked by wounding and application of *S. exigua* regurgitant. Fold changes compared with nonelicited controls are shown. Stars indicate significant differences in inducibility between B73 and P39 (n = 5, ±se, Student's *t* test, P < 0.05). Dashed lines indicate trait differences that were used for QTL mapping.

2.09, and 4.03, respectively; Figure 2A; Supplemental Table 3). By contrast, the HDM₂BOA-Glc mapping resulted in two QTLs on chromosome 2, which were identical to *Bb1* and *Bb2* (Figure 2B). On average, each of the identified QTLs covered ~900 putative coding DNA sequences.

In contrast to inbred line P39, which produced the largest leaf amounts of DIM₂BOA-Glc among all the tested NAM parental lines, inbred line Oh43 accumulated no detectable amounts of this compound (Figure 1A). We therefore mapped the constitutive production of DIM₂BOA-Glc in the B73 × Oh43 recombinant inbred population. The mapping identified one QTL on chromosome 2 that was identical to *Bb2* (Figure 2C; Supplemental Table 3).

Differences in root DIM₂BOA-Glc content between the B73 and Mo17 NAM lines (Figure 1A) allowed us to use the Mo17 × B73

population for mapping DIM₂BOA-Glc concentration in the roots. This experiment also revealed the QTL *Bb2* on chromosome 2 (Figure 2D; Supplemental Table 3). Although HDM₂BOA-Glc concentrations in B73 and Mo17 roots were not significantly different (Figure 1A), there is transgressive segregation for this trait and genetic mapping with the B73 × Mo17 population identified the *Bb1* and *Bb2* loci (Figure 2E), as in the case of the B73 × P39 mapping population (Figure 2B). To gain insight into the genetic control of herbivore-induced formation of HDM₂BOA-Glc, we mapped the concentration of this compound in *S. exigua*-induced leaf sections of the B73 × P39 population. Again, as in all previous mapping experiments, a major QTL identical to *Bb2* was mapped (Figure 2F; Supplemental Table 3), suggesting that *Bb2* is required for the formation of both constitutive DIM₂BOA-Glc and herbivore-induced HDM₂BOA-Glc.

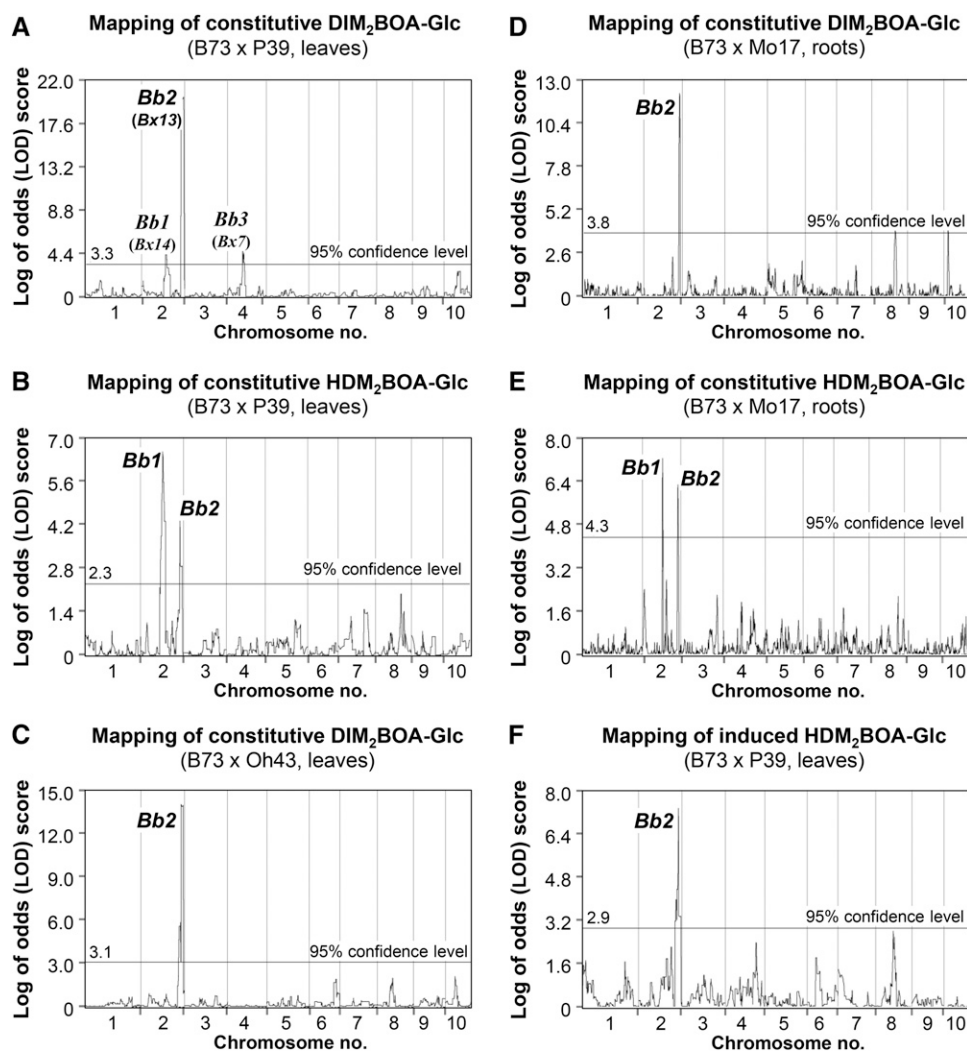


Figure 2. QTL Mapping of Constitutive and Herbivore-Induced Content of DIM₂BOA-Glc and HDM₂BOA-Glc in Different RIL Populations.

Constitutive DIM₂BOA-Glc content was mapped using the B73 × P39 (A), B73 × Oh43 (C), and B73 × Mo17 (D) RIL populations and resulted in three benzoxazinoid biosynthesis QTLs, *Bb1* to 3, on chromosomes 2 and 4. Mapping of constitutive HDM₂BOA-Glc levels using the B73 × P39 RIL population (B) and B73 × Mo17 population (E) resulted in *Bb1* and *Bb2*. Mapping of HDM₂BOA-Glc abundance (F) in herbivory-induced leaves also resulted in *Bb2*.

The QTL *Bb2* Contains a Candidate Dioxygenase Gene, *Bx13*

Given that the formation of the core benzoxazinoid, DIMBOA-Glc, might follow a linear pathway (Frey et al., 2009; Meihls et al., 2013), we hypothesized that DIM₂BOA-Glc is produced from DIMBOA-Glc via hydroxylation of the aromatic ring at C-8 and subsequent methylation of the hydroxyl group. Such a reaction sequence is analogous to the formation of DIMBOA-Glc from DIBOA-Glc, which has been shown to involve the hydroxylation of the aromatic ring at C-7 and the methylation of the resulting hydroxyl group, catalyzed by the 2ODD BX6 and the O-methyltransferase (OMT) BX7, respectively (Jonczyk et al., 2008). While two of the identified QTLs, *Bb1* and *Bb3*, contain at least one putative OMT gene, only one QTL, *Bb2*, contained a putative 2ODD gene (AC148152.3_FG005). Since a sequence comparison with maize 2ODDs similar to AC148152.3_FG005 revealed that the mapped 2ODD gene clustered with *Bx6* (Figure 3A; Supplemental Data Set 1), we hypothesized that AC148152.3_FG005 encodes the first enzymatic step in the formation of DIM₂BOA-Glc from DIMBOA-Glc.

BX13 Catalyzes the Oxidation of DIMBOA-Glc to TRIMBOA-Glc

To test the enzymatic activity of AC148152.3_FG005, we heterologously expressed the P39 allele in *Escherichia coli*. Enzyme assays containing the purified protein, the potential substrate DIMBOA-Glc, and the cosubstrate 2-oxoglutarate resulted in the formation of a single product, while a control assay containing the nickel affinity-purified protein fraction from *E. coli* expressing the empty vector showed no product formation (Figure 3B). Liquid chromatography-tandem mass spectrometry (LC-MS/MS) analysis of the enzyme product revealed a fragmentation pattern consistent with an oxidized DIMBOA-Glc (Supplemental Figure 2). Activity assays with HDMBOA-Glc showed that AC148152.3_FG005 was not able to accept this compound as substrate (Supplemental Figure 3). Notably, BX6, which shares 77% identity at the amino acid level to AC148152.3_FG005, showed no activity with DIMBOA-Glc (Supplemental Figure 3). Due to the catalytic activity of AC148152.3_FG005, we renamed the enzyme BX13, following the nomenclature for enzymes involved in benzoxazinoid biosynthesis (Frey et al., 2009).

To isolate the DIMBOA-Glc oxidation product for NMR analysis, 300 enzyme assays were performed and pooled. Product purification was done using semipreparative HPLC, resulting in ~100 µg of pure compound. While the NMR measurements confirmed the known structure of the BX13 substrate DIMBOA-Glc, containing a methoxy group at C-7 of the aromatic ring, NMR analysis of the enzyme product revealed an unexpected structure, 2-(2,4,7-trihydroxy-8-methoxy-1,4-benzoxazin-3-one)-β-D-glucopyranose (TRIMBOA-Glc; Supplemental Table 4), with a hydroxyl group at C-7 and a methoxy group at C-8 of the aromatic ring (Figure 3C).

The DIM₂BOA-Glc-Free Inbred Line Oh43 Possesses a Mutated Allele of *Bx13*

In the NAM parental population, Oh43 was the only inbred line lacking any detectable amounts of DIM₂BOA-Glc and HDM₂BOA-Glc (Figure 1). A nucleotide sequence alignment of *Bx13*-P39 with genomic Oh43 Illumina sequences (SRX119503; <http://blast.ncbi.nlm.nih.gov>) revealed allelic variation within the *Bx13* start codon (*Bx13*-P39, ATG; *Bx13*-Oh43, TTT; Figure 4A; Supplemental Figure 4). To verify this mutation, we sequenced the complete *Bx13* open reading frame amplified from Oh43 cDNA. Since there was a second in-frame start codon 41 codons downstream from the first ATG, the mutation of the Oh43 allele presumably results in a shorter open reading frame encoding a protein that lacks the first 41 amino acids (Supplemental Figures 3 and 4). Although alignments with crystallized plant 2ODD sequences revealed that the putative active site was unaffected by the truncation (Supplemental Figure 5), truncated recombinant BX13-Oh43 showed no enzymatic activity with DIMBOA-Glc (Figure 4B).

To discover other naturally occurring *Bx13* knockout variants, we performed sensitive remapping of Illumina reads from 916 diverse maize lines in HapMap 3.1 (Bukowski et al., 2015). This approach, in combination with PCR amplification and resequencing, revealed that two inbred lines, LH38 and LH39, contain the same start codon mutation as *Bx13*-Oh43 (Supplemental Figure 6A). Benzoxazinoid analysis confirmed that LH38 and LH39 do not accumulate DIM₂BOA-Glc and HDM₂BOA-Glc (Supplemental Figure 6B).

To discover other naturally occurring *Bx13* knockout variants, we performed sensitive remapping of Illumina reads from 916 diverse maize lines in HapMap 3.1 (Bukowski et al., 2015). This approach, in combination with PCR amplification and resequencing, revealed that two inbred lines, LH38 and LH39, contain the same start codon mutation as *Bx13*-Oh43 (Supplemental Figure 6A). Benzoxazinoid analysis confirmed that LH38 and LH39 do not accumulate DIM₂BOA-Glc and HDM₂BOA-Glc (Supplemental Figure 6B).

Near Isogenic Maize Lines Differing in the *Bx13* Locus Vary in DIM₂BOA-Glc and HDM₂BOA-Glc Levels

To test the activity of BX13 in planta, we generated near isogenic lines (NILs) possessing either the B73 allele or the Oh43 allele of *Bx13*. Line Z022E0081 from the B73 × Oh43 recombinant inbred line (RIL) population, which is heterozygous for *Bx13* was selfed, 37 F₂ progeny plants were genotyped at *Bx13* and other previously heterozygous genomic loci (Supplemental Table 5 and Supplemental Figure 7), and homozygous, near-isogenic *Bx13*-B73 and *Bx13*-Oh43 lines were identified. The variable segment in this NIL pair constitutes <0.5% of the maize genome (~4.7 Mb and 185 genes). Constitutive and herbivore-induced formation of benzoxazinoids was measured in the identified homozygous lines. While the NIL carrying *Bx13*-B73 (*Bx13*NIL-B73) produced DIM₂BOA-Glc and HDM₂BOA-Glc in comparable amounts to B73, the NIL carrying *Bx13*-Oh43 (*Bx13*NIL-Oh43) contained no detectable DIM₂BOA-Glc and HDM₂BOA-Glc (Figure 4C). By contrast, DIMBOA-Glc and HDMBOA-Glc showed no significant differences between the parental lines and the NILs (Figure 4C).

The QTL *Bb3* Comprises the O-Methyltransferase Gene *Bx7*, Which Encodes an Enzyme Accepting TRIMBOA-Glc as Substrate

The formation of DIM₂BOA-Glc from TRIMBOA-Glc requires methylation of the C-7 hydroxyl group, likely catalyzed by an O-methyltransferase. The QTLs *Bb1* and *Bb3*, which appeared in the DIM₂BOA-Glc mapping (Figure 2A), contain seven sequences annotated as OMTs, including *Bx7*. Since BX7 methylates the C-7 hydroxyl group of TRIMBOA-Glc (Jonczyk et al., 2008), we hypothesized that it could also catalyze the methylation of the corresponding hydroxyl group of TRIMBOA-Glc. To test this hypothesis, *Bx7* was heterologously expressed in *E. coli* and the purified recombinant protein was assayed with TRIMBOA-Glc as substrate and S-adenosyl-L-methionine as cosubstrate. While an empty

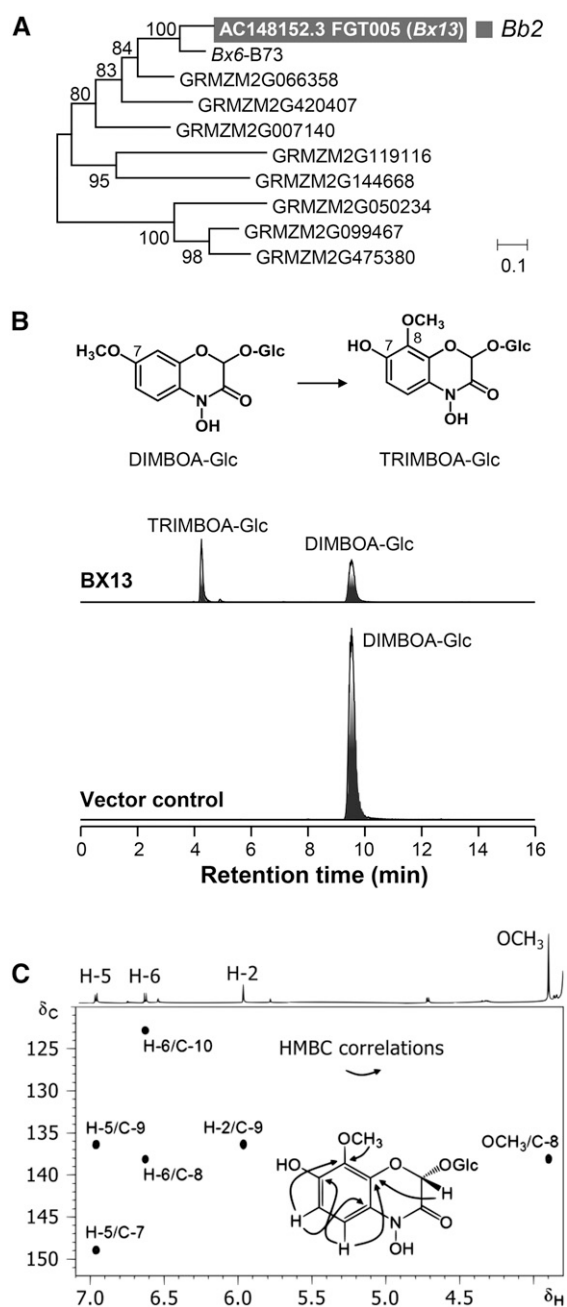


Figure 3. Identification, Characterization, and Product Identification of BX13.

(A) Dendrogram analysis (unrooted tree) of maize *2ODD* genes similar to *Bx6-B73*. The tree was inferred using the maximum likelihood method and $n = 1000$ replicates for bootstrapping. Bootstrap values are shown next to each node. The tree is drawn to scale, with branch lengths measured in the number of substitutions per site. The candidate gene that has been mapped on chromosome 2 (QTL *Bb2*) is marked in gray. The alignment is available in Supplemental Data Set 1.

(B) Purified recombinant BX13 as well as the empty vector control were incubated with DIMBOA-Glc and the cofactors Fe(II) and 2-oxoglutarate. Product formation was analyzed by LC-MS/MS. The relative intensities of the LC-MS/MS transitions are shown.

vector control showed no product formation, recombinant BX7 produced significant amounts of DIM₂BOA-Glc (Figure 5; Supplemental Data Set 2 and Supplemental Figure 8).

Dendrogram analysis of the seven putative OMT genes located in the QTLs *Bb1* and *Bb3* showed that two sequences, GRMZM2G127418 and GRMZM2G023152, were similar to BX7 (Figure 5A). We therefore expressed these genes in *E. coli* to test whether they also methylate TRIMBOA-Glc. However, GRMZM2G127418 and GRMZM2G023152 showed no activity with this substrate (Supplemental Figure 8). Four other OMT genes, including GRMZM2G423027, GRMZM2G078143, GRMZM2G078548, and the previously characterized *Zm-Omt1*, which encodes tricetin *O*-methyltransferase (Zhou et al., 2008), belong to other OMT families and were thus not considered as benzoxazinoid-producing candidates.

Since *Bx7* is part of a small gene family consisting of 15 members with higher sequence similarity to each other (62 to 99%; Figure 5A), we tried to amplify all remaining potential OMT candidates and tested them for TRIMBOA-Glc OMT activity. However, only GRMZM2G097297, GRMZM2G100754, AC209819.3 FG005, *ZRP4*, *Bx10*, *Bx11*, and *Bx12* could be obtained from cDNA and none of them catalyzed the conversion of TRIMBOA-Glc into DIM₂BOA-Glc (Supplemental Figure 8). Synthesized sequences for GRMZM2G093092 and GRMZM2G106172 were expressed in *E. coli*, but the recombinant proteins showed no activity with TRIMBOA-Glc (Supplemental Figure 8).

BX14, an *O*-Methyltransferase from the QTL *Bb1*, Converts DIM₂BOA-Glc into HDM₂BOA-Glc

We identified two putative OMT genes in the confidence interval of *Bb1*, the QTL with the highest LOD score for constitutive HDM₂BOA-Glc production (Figure 5A). A multiple alignment revealed that one of them, GRMZM2G127418, showed high nucleotide sequence identity to *Bx10* (87.5%), *Bx11* (87.4%), and *Bx12* (86.9%), which have been shown to encode enzymes that catalyze the conversion of DIMBOA-Glc into HDMBOA-Glc (Meihls et al., 2013). The second OMT candidate in the *Bb1* QTL interval, GRMZM2G078548, clustered separately from the benzoxazinoid-specific OMT genes and showed only ~35% nucleotide identity to *Bx10-12* and 34% nucleotide identity to *Bx7* (Figure 5A).

To test for benzoxazinoid-specific OMT activity, GRMZM2G127418 was amplified from B73 leaf cDNA and heterologously expressed in *E. coli*. The enzyme was purified and incubated with the potential substrate DIM₂BOA-Glc and the cosubstrate *S*-adenosyl-L-methionine. Subsequent LC-MS/MS analysis revealed the formation of HDM₂BOA-Glc, while the empty vector control showed no substrate turnover (Figure 5C). Therefore, GRMZM2G127418 was designated as BX14. In addition to DIM₂BOA-Glc, recombinant BX14 also accepted DIMBOA-Glc and produced HDMBOA-Glc, while it showed no activity with TRIMBOA-Glc

(C) Partial HMBC spectrum (500 MHz) of TRIMBOA-Glc displaying correlation signals between protons and carbon atoms of the aglucone through three bonds. The OCH₃/C-8 cross signal verifies the position of the *O*-methyl group at C-8.

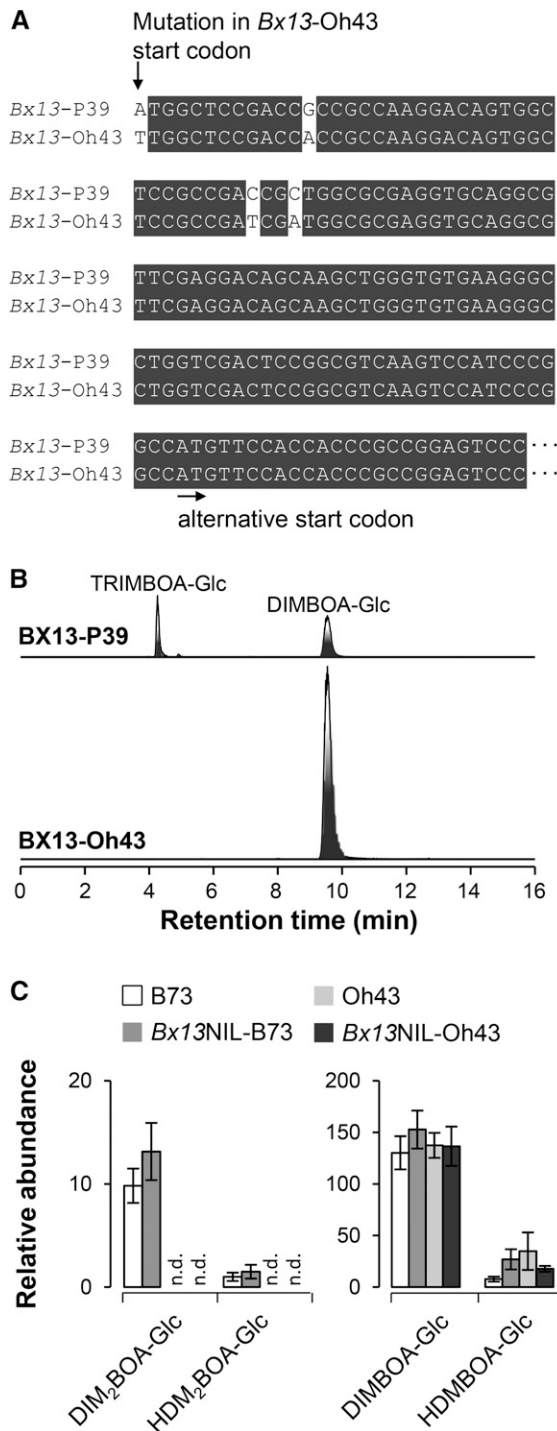


Figure 4. A Mutation in the *Bx13* Allele from the Inbred Line Oh43 Causes Loss of Enzyme Activity *In Vitro* and *In Vivo*.

(A) Sequence alignment of *Bx13*-P39 and *Bx13*-Oh43. The two arrows indicate the start codon mutation of the Oh43 allele and the alternative start codon, respectively. The complete alignment is shown in Supplemental Figure 4.

(B) Activity assays of purified enzymes incubated with DIMBOA-Glc, the cofactor Fe(II), and 2-oxoglutarate. Shown are the relative intensities of the specific LC-MS/MS transitions.

(Supplemental Figure 8). Other OMTs with high similarity to BX14, including BX7, BX10, BX11, BX12, ZRP4, AC209819.3_FG005, GRMZM2G099297, GRMZM2G106172, and GRMZM2G093092 (Figure 5A), were not able to convert DIM₂BOA-Glc into HDM₂BOA-Glc (Supplemental Figure 9).

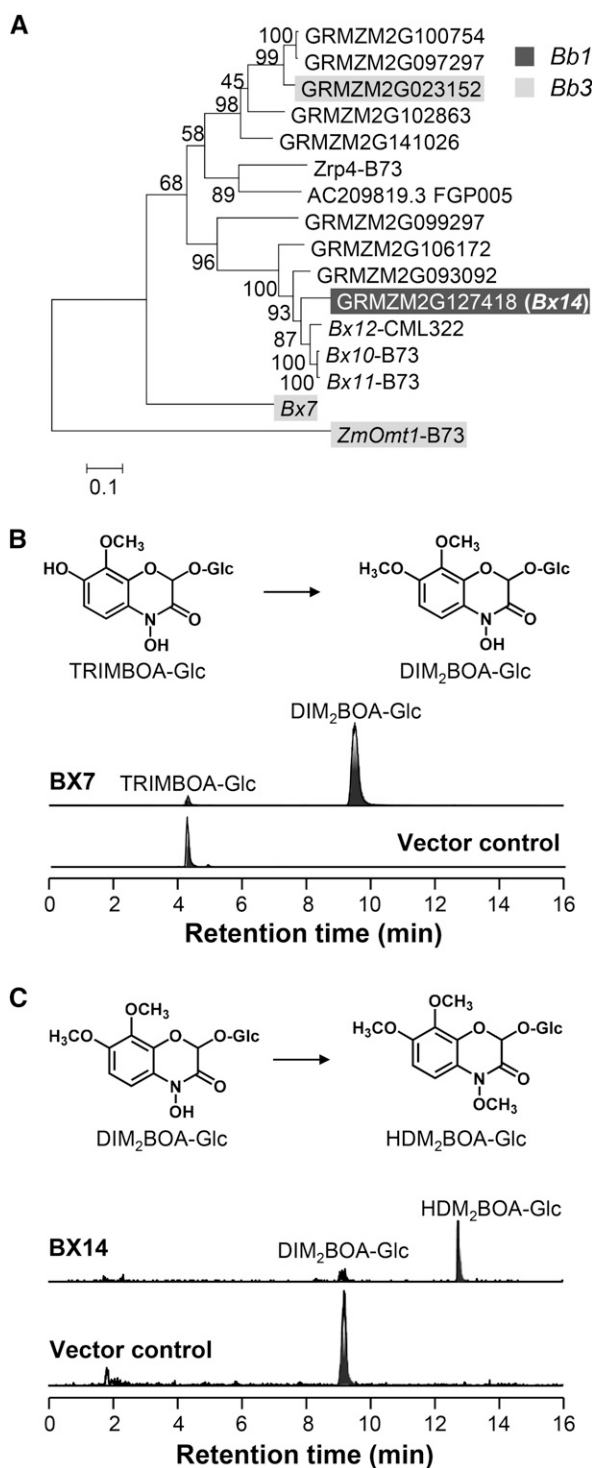
The Inbred Line Il14H Possesses an Inactive *Bx14* Allele and Is Not Able to Produce HDM₂BOA-Glc in the Leaves

Analysis of benzoxazinoids in the NAM parental lines showed that four of the tested lines produced no detectable amounts of HDM₂BOA-Glc but accumulated its potential precursor DIM₂BOA-Glc (Figure 1B). Since such a phenotype might be explained by an inactive *Bx14* allele, we performed a sequence comparison of *Bx14*-P39 with genomic Illumina sequences from the HDM₂BOA-Glc nonproducing inbred line Il14H (SRP011907; <http://blast.ncbi.nlm.nih.gov>). In addition to several single nucleotide polymorphisms, the resulting alignment showed an in-frame insertion of 30 bp in the *Bx14*-Il14H allele leading to an extended open reading frame (Supplemental Figure 10). These mutations could be confirmed by sequencing of *Bx14*-Il14H amplified from cDNA. Activity assays with purified recombinant BX14-Il14H revealed that the enzyme did not accept DIM₂BOA-Glc as substrate (Supplemental Figure 11). PCR analysis of genomic DNA prepared from the 25 NAM parental inbred lines showed that the 30-bp insertion occurred in multiple *Bx14* alleles but was not correlated with the presence or absence of HDM₂BOA-Glc (Supplemental Figure 11). This indicates that most likely other point mutations, rather than the 30-bp insertion, caused the inactivity of the Il14H allele. Interestingly, we detected small amounts of HDM₂BOA-Glc in the roots of Il14H (Figure 1B). It is therefore likely that an additional OMT contributes to the production of this metabolite in Il14H roots.

The Inducibility of HDM₂BOA-Glc Is Associated with a Stronger Induction of *Bx13* and *Bx14* in P39

Compared with B73, the inbred line P39 produced higher constitutive levels of DIM₂BOA-Glc and accumulated higher levels of HDM₂BOA-Glc after simulated herbivory (Figures 1A and 1C). To test whether variation in gene expression can explain these differences, we analyzed transcript accumulation of *Bx7*, *Bx13*, and *Bx14* in undamaged and damaged (mechanical damage + *S. exigua* oral secretion) leaves of P39 and B73 seedlings. *Bx7* was constitutively expressed in both lines and showed no significant increase in transcript accumulation after simulated herbivory. Notably, constitutive *Bx7* expression was significantly higher in P39 than in B73 (Figure 6A). *Bx13* and *Bx14* were significantly upregulated upon simulated herbivory in both inbred lines and showed significantly higher constitutive transcript accumulation in P39 in comparison to B73 (Figures 6B and 6C).

(C) Relative benzoxazinoid content in leaf extracts of the maize inbred lines B73 and Oh43, as well as of near isogenic lines possessing either the B73 allele of *Bx13* (*Bx13*NIL-B73) or the Oh43 allele of *Bx13* (*Bx13*NIL-Oh43). DIM₂BOA-Glc and HDM₂BOA-Glc could not be detected (n.d.) in leaves of the inbred Oh43 and the near isogenic line *Bx13*NIL-Oh43 ($n = 5$, \pm SE).



BX13 Activity Has Weak Effects on the Induction and Activation of Other Benzoxazinoids

To assess the suitability of the two *Bx13* NILs (Figure 4C) for biological experiments, we first verified whether the inactivation of *Bx13* affects the constitutive and herbivore-induced biosynthesis and deglycosylation of benzoxazinoids in the leaves (Supplemental Figure 12). For this purpose, we incubated ground maize leaves at room temperature for 0 to 10 min and measured benzoxazinoid glucosides and aglucones. As expected, DIM₂BOA-Glc and HDM₂BOA-Glc were only present in the *Bx13*NIL-B73. Repeated measures analysis of variance showed no significant genotype or genotype:time interaction effects for the other benzoxazinoids (Supplemental Table 6). Pairwise comparisons revealed slightly elevated levels of HBOA-Glc and DIMBOA-Glc in *S. frugiperda* attacked *Bx13*NIL-B73 compared with *Bx13*NIL-Oh43 plants (Supplemental Figure 12). Furthermore, 3 to 10 min after tissue disruption, elevated levels of DIMBOA and MBOA were observed. These data suggest that *Bx13* inactivation has weak negative feedback effects on benzoxazinoid abundance and activation in herbivore attacked plants. Alternatively, the differential accumulation may be the result of changes in *S. frugiperda* behavior (see below).

The Performance of Chewing Herbivores Is Not Affected by *Bx13*

To understand the impact of HDM₂BOA-Glc and DIM₂BOA-Glc on the interaction between maize and chewing herbivores, we conducted several experiments. First, we offered pairs of *Bx13*NIL-Oh43 and *Bx13*NIL-B73 to fall armyworm larvae and recorded their feeding patterns. Surprisingly, the larvae caused more damage on *Bx13*NIL-B73 (Figure 7A) and were more often found on this genotype (Figure 7B). Larval weight gain did not differ between the two NILs in a no-choice experiment (Figure 7C). As the fall armyworm is well adapted to maize defenses and is known to use benzoxazinoids as foraging cues (Glauser et al., 2011; Köhler et al., 2015), we performed additional experiments with two generalist leaf feeders, the beet armyworm (*S. exigua*) and the Egyptian cotton leafworm. As HDM₂BOA-Glc and DIM₂BOA-Glc levels are higher in B73 roots than the leaves (Figure 1), we also tested the effect of *Bx13* inactivation on the banded cucumber beetle *Diabrotica balteata*, a generalist herbivore known to feed on maize. All tested herbivores gained the same amount of weight on *Bx13*NIL-B73 and *Bx13*NIL-Oh43 (Figure 7D), suggesting that HDM₂BOA-Glc and DIM₂BOA-Glc do not increase plant resistance against these chewing insects.

site. Genes that have been mapped on chromosome 2 (QTL *Bb1*) are marked in dark gray, and genes located in the QTL *Bb3* on chromosome 4 are highlighted in light gray. The alignment is available in Supplemental Data Set 2.

(B) and **(C)** Activity assays of purified recombinant enzymes as well as the empty vector control incubated with the respective substrate and the co-substrate *S*-adenosyl-L-methionine. The relative intensities of the specific LC-MS/MS transitions (see Methods) are shown.

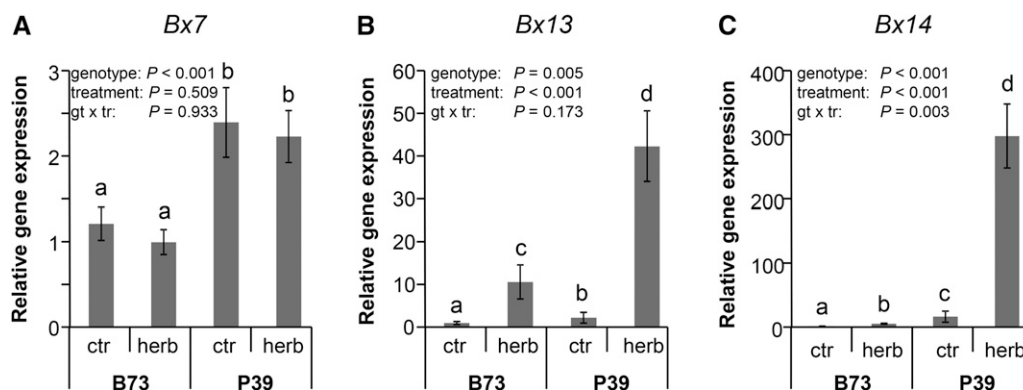


Figure 6. Transcript Accumulation of *Bx7*, *Bx13*, and *Bx14* in Maize Leaves upon Simulated Herbivory.

Gene expression of *Bx7*, *Bx13*, and *Bx14* in undamaged (ctr) and wounded (mechanical damage + *S. exigua* oral secretion [herb]) leaves of the maize inbred lines B73 and P39 was measured using qRT-PCR relative to *actin1* (means \pm SE; $n = 7$ biological replicates). Significance levels of a two-way ANOVA are shown for the factors “genotype,” “treatment,” and the interaction term (genotype \times treatment). Different letters indicate significant differences between genotypes and treatments.

Bx13 Decreases Aphid Reproduction

To test whether HDM₂BOA-Glc and DIM₂BOA-Glc affect the performance of phloem feeders, we conducted a performance experiment with maize leaf aphids (*Rhopalosiphum maidis*). Seven days after the start of the experiment, the survival of adult aphids was not significantly different on *Bx13*NIL-B73 and *Bx13*NIL-Oh43 maize seedlings ($P = 0.3$ and $P = 0.65$, Student’s *t* test of two independent experiments). However, aphids feeding on *Bx13*NIL-Oh43 produced 50% more progeny than aphids feeding on *Bx13*NIL-B73 (Figure 8; Supplemental Figure 13), suggesting that HDM₂BOA-Glc and/or DIM₂BOA-Glc accumulation increases aphid resistance.

DISCUSSION

Maize produces a number of benzoxazinoids that defend the plant against insect herbivores and pathogens (Oikawa et al., 2004; Glauser et al., 2011; Ahmad et al., 2011; Meihls et al., 2013; Maag et al., 2014). The biosynthetic pathway leading to DIMBOA-Glc, the most abundant benzoxazinoid in maize, has been fully determined (Frey et al., 1997; von Rad et al., 2001; Jonczyk et al., 2008). However, how DIMBOA-Glc is converted into other benzoxazinoids is not well understood. Here, we investigated the biosynthesis and biological relevance of the 8-*O*-methylated benzoxazinoids, DIM₂BOA-Glc and HDM₂BOA-Glc.

The Dioxygenase *BX13* Is the Key Enzyme for the Formation of DIM₂BOA-Glc and HDM₂BOA-Glc

BX13 belongs to the 2-oxoglutarate-dependent dioxygenase superfamily and has been classified as a member of the recently defined DOXC class of 2ODDs, encompassing enzymes known to be involved in specialized metabolism (Kawai et al., 2014). Several lines of evidence indicated that *BX13* acts as the key enzyme for the formation of DIM₂BOA-Glc and HDM₂BOA-Glc in planta: First, both constitutive DIM₂BOA-Glc levels and constitutive and

induced HDM₂BOA-Glc levels mapped to the same major QTL (*Bb2*) on chromosome 2 that includes the *Bx13* gene, in experiments with several different RIL populations (Figure 2; Supplemental Table 3). Second, a natural knockout of *Bx13*, attributed to a mutated start codon in the inbred lines Oh43, LH38, and LH39, was correlated with a complete lack of DIM₂BOA-Glc and HDM₂BOA-Glc (Figure 1; Supplemental Figures 4 and 5) and analysis of near-isogenic lines differing mostly in the *Bx13* locus showed that a line carrying the mutated and inactive Oh43 allele produced no DIM₂BOA-Glc and HDM₂BOA-Glc (Figure 4C). Third, recombinant *BX13* was able to convert DIMBOA-Glc to TRIMBOA-Glc (Figure 3B), while *BX6* could not accept DIMBOA-Glc as substrate (Supplemental Figure 3A). Other routes to HDM₂BOA-Glc could be ruled out since neither *BX13* nor *BX6* accepted HDMBOA-Glc as substrate (Supplemental Figure 3B). Moreover, none of the tested OMTs were able to methylate the hydroxyl group of the hydroxamic acid moiety of TRIMBOA-Glc (Supplemental Figure 8). Taken together, our findings demonstrate that the formation of DIM₂BOA-Glc and HDM₂BOA-Glc from DIMBOA-Glc most likely follows a linear pathway beginning with the conversion of DIMBOA-Glc into TRIMBOA-Glc catalyzed by *BX13* (Figure 9).

BX13 Catalyzes an Unusual Reaction That Likely Involves an Ortho-Rearrangement of the Methoxy Group

Contrary to our initial expectation that the *BX13*-catalyzed hydroxylation of DIMBOA-Glc would result in a compound possessing the hydroxyl group at C-8 next to the preexisting methoxy group at C-7, NMR analysis of the enzyme product TRIMBOA-Glc revealed the opposite configuration with a hydroxyl group at C-7 and a methoxy group at C-8 (Figure 3C). This finding can be explained by a C-7 hydroxylation and a subsequent 1,2-shift of the methoxy group catalyzed by the enzyme. Indeed, 4-hydroxyphenylpyruvate dioxygenase (HPPD), a member of the 2ODD superfamily that does not use 2-oxoglutarate as a cofactor, is known to catalyze an oxidation of an aromatic ring and a subsequent ortho-rearrangement of an acetate side chain (Raspail et al., 2011).

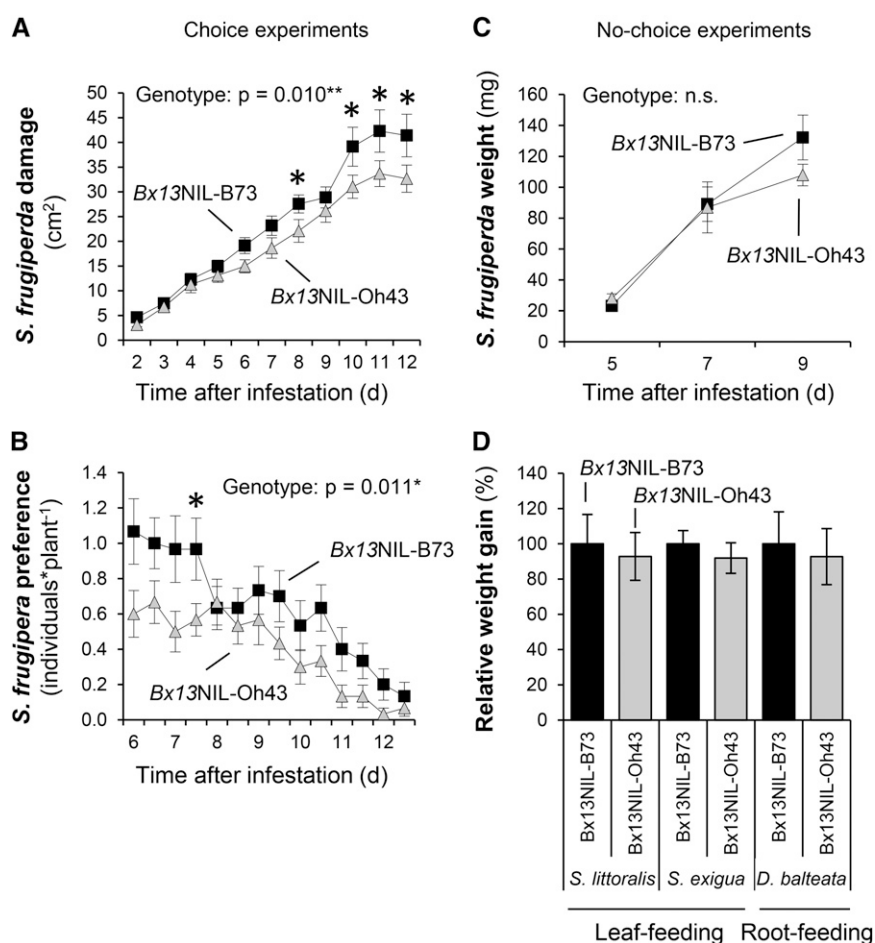


Figure 7. BX13 Increases the Attractiveness of Maize Plants to *S. frugiperda*, but Does Not Affect the Performance of *S. frugiperda* and Other Insects.

(A) and (B) Damage (A) and distribution (B) of *S. frugiperda* caterpillars on the *Bx13* mutant (*Bx13NIL-Oh43*) and its near-isogenic wild-type line (*Bx13NIL-B73*) in choice experiments. Caterpillars were released into pots containing one plant of each genotype and left to feed for 12 d ($n = 30$, \pm SE).

(C) *S. frugiperda* weight gain in a no-choice experiment ($n = 18$, \pm SE). Caterpillars were left to feed on individual plants for 9 d. Stars indicate significant differences between genotypes at individual time points. Significant P values for overall genotype effects from ANOVA are shown.

(D) Relative weight gain of three generalist herbivores feeding between 6 and 10 d on the leaves or roots of the two genotypes. For comparative purposes, weight gains are expressed in percentages relative to weight gain on *Bx13NIL-B73* (*S. littoralis*, $n = 7$ to 9; *S. exigua*, $n = 38$ to 52; *D. balteata*, $n = 8$).

HPPD accepts 4-hydroxyphenylpyruvate as substrate and converts it into homogentisate, an essential intermediate in plastoquinone and tocopherol biosynthesis in plants (He and Moran, 2009; Goodwin and Mercer, 1983). We propose that the formation of TRIMBOA-Glc by BX13 might follow a reaction mechanism similar to that described for HPPD (Figure 10). The active site of BX13 contains two highly conserved histidines and one aspartate residue (Supplemental Figure 5) that can form a complex with iron and 2-oxoglutarate (Schofield and Zhang, 1999). After binding of molecular oxygen and DIMBOA-Glc, the activated dioxygen can attack the side chain of the 2-oxoglutarate, leading to its decarboxylation. Then, C-7 hydroxylation of DIMBOA-Glc occurs via an electrophilic attack by an Fe-oxene. A subsequent 1,2-shift of the methoxy group favored by the positive charge at C-8 results in the formation of TRIMBOA-Glc (Figure 10). Although the proposed mechanism explains the production of TRIMBOA-Glc, we cannot rule out the

possibility that hydroxylation of DIMBOA-Glc might alternatively occur at C-8 followed by a transfer of the methyl group from the methoxy group to the newly incorporated 8'-OH group. There are a few examples of plant 2ODDs possessing O-demethylation activity (Hagel and Facchini, 2010; Berim et al., 2015). However, a 2ODD-catalyzed transfer of a methyl group between two substrate OH groups has to our knowledge not been reported so far. To further study the reaction mechanism of BX13 and to discriminate between a methoxy group rearrangement and an alternative methyl group transfer, enzyme assays with either labeled DIMBOA-Glc or ¹⁸O₂, respectively, are planned for future experiments.

The Role of BX7 and BX14 in HDM₂BOA-Glc Formation

BX7 has been described to catalyze the methylation of the 7-OH group of TRIBOA-Glc (Jonczyk et al., 2008). As discussed

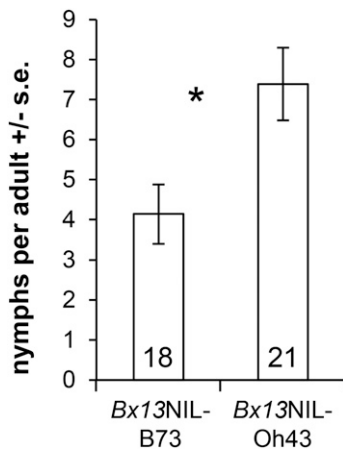


Figure 8. *Bx13* Decreases Aphid Performance.

The number of nymphs per adult on the *Bx13* mutant (*Bx13NIL-Oh43*) and its near-isogenic wild-type line (*Bx13NIL-B73*) is shown ($n = 20, \pm \text{SE}$). Stars indicate significant differences between genotypes ($P < 0.05$, Student's *t* test). Numbers in bars = sample sizes.

above, the resulting DIMBOA-Glc can act as a substrate for *Bx13*. Due to the unusual reaction of this 2ODD, the enzyme product TRIMBOA-Glc possesses a free hydroxyl group at C-7 similar to TRIBOA-Glc (Figure 3C). We showed that recombinant *Bx7* also accepted TRIMBOA-Glc as substrate and methylated the hydroxyl group at C-7 (Figure 5B). Since all other tested potential OMT candidates were not able to catalyze this reaction (Figure 5A; Supplemental Figure 8), we assume that *Bx7* catalyzes the *O*-methylations of both TRIBOA-Glc and TRIMBOA-Glc in planta. It is notable that neither of the *Bx7* substrates, TRIBOA-Glc and TRIMBOA-Glc, were found to accumulate in the plant, indicating a rapid turnover by the enzyme. *Bx7* is similar to other plant OMTs acting on polyhydroxylated small molecules such as phenylpropanoids and their derivatives (Meihls et al., 2013; Zubieta et al., 2001). In general, the majority of enzymes belonging to this OMT group possess high substrate and positional specificity (Ibrahim, 1997; Zubieta et al., 2001). However, a few enzymes such as caffeic acid *O*-methyltransferase demonstrate greater substrate promiscuity (Zubieta et al., 2001). Although *Bx7* seems to have high positional specificity toward the hydroxyl group at C-7, catalytic activity is not influenced by the presence or absence of the neighboring methoxy group, indicating moderate spatial flexibility of the active site.

The *O*-methyltransferase *Bx14* showed high similarity to the recently described DIMBOA-Glc *O*-methyltransferases *Bx10*, *Bx11*, and *Bx12* (Meihls et al., 2013) and catalyzed the same reaction as already described for *Bx10-12* (Supplemental Figure 9A). While *Bx10-12* possessed high substrate specificity toward DIMBOA-Glc (Supplemental Figure 9A), *Bx14* also accepted DIM₂BOA-Glc as substrate and produced HDM₂BOA-Glc (Figure 5C). A dendrogram analysis suggests that *Bx10*, *Bx11*, and *Bx12* are likely derived by gene duplication of a *Bx14*-related ancestor (Figure 5A).

Natural Variation in *Bx7*, *Bx13*, and *Bx14* Expression

It has been shown that genes of the core benzoxazinoid pathway including *Bx1*, *Bx2*, *Bx3*, *Bx4*, *Bx5*, *Bx6*, and *Bx8* are located in close proximity to each other on the short arm of maize

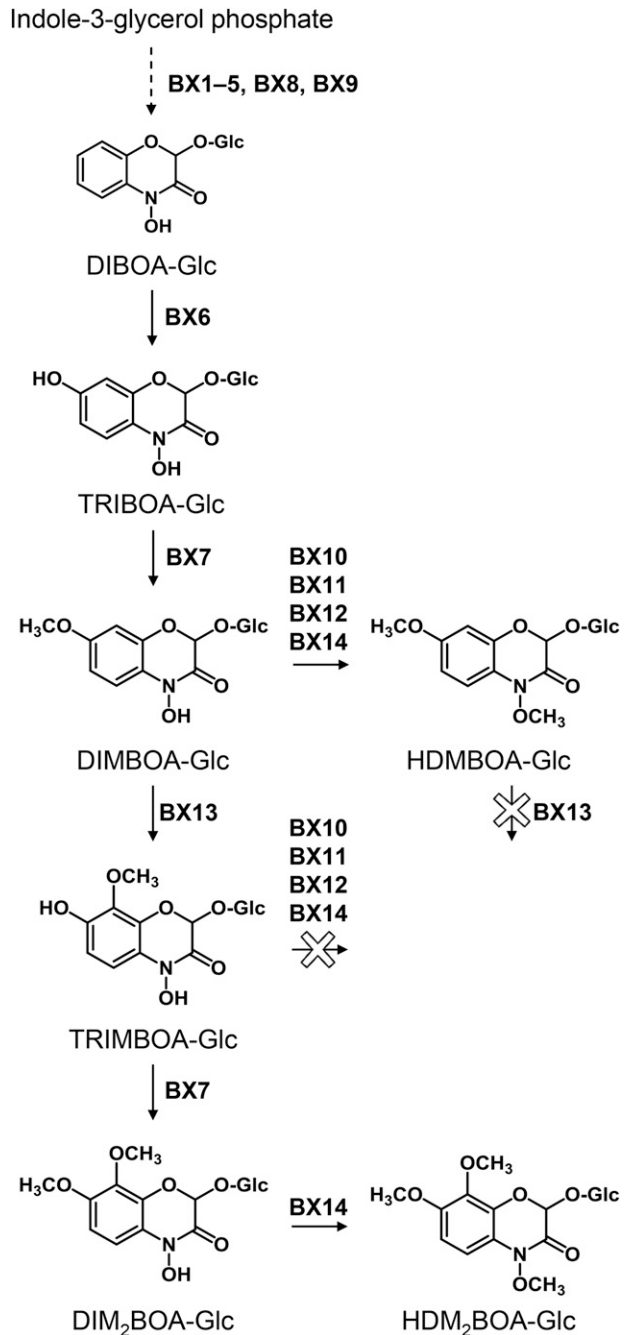


Figure 9. The Later Steps of Benzoxazinoid Formation in Maize.

The formation of DIMBOA-Glc (the major benzoxazinoid in maize) and HDMBOA-Glc originating from indole-3-glycerol phosphate have been reported earlier. The 8-*O*-methylated DIM₂BOA-Glc and HDM₂BOA-Glc are formed from DIMBOA-Glc by *Bx13*, *Bx7*, and *Bx14*.

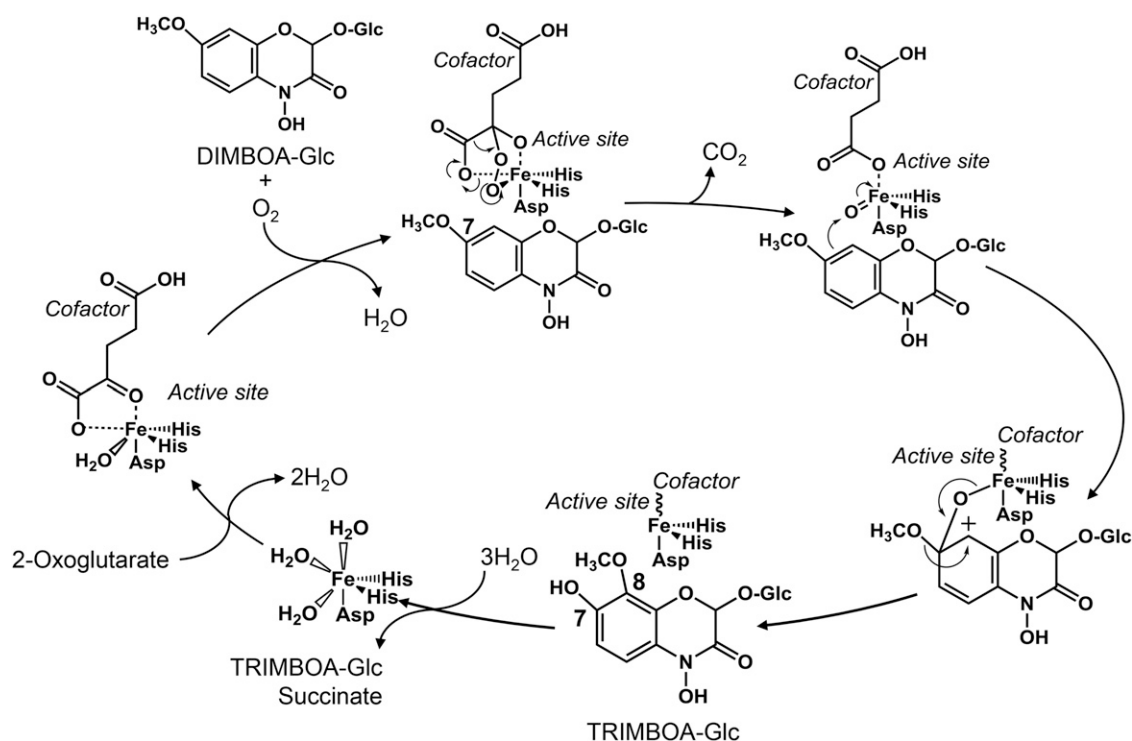


Figure 10. Proposed Reaction Mechanism for the Formation of TRIMBOA-Glc from DIMBOA-Glc Catalyzed by BX13.

An initial oxidation of the C-7 methoxy group of DIMBOA-Glc might be followed by the elimination and simultaneous, aromatic ring substitution of the leaving moiety at position 8, resulting in TRIMBOA-Glc.

chromosome 4 (Frey et al., 2009). In general, such an organization of functionally related genes in operon-like gene clusters in plants is considered to facilitate the coregulation of gene expression (Jonczyk et al., 2008; Osbourn, 2010), which, however, would imply less regulatory flexibility at the single gene level. While DIMBOA-Glc is mainly produced in young seedlings 4 to 6 d after germination and declines thereafter, the production of HDMBOA-Glc and HDM₂BOA-Glc also occurs in older tissues (Cambier et al., 2000; Köhler et al., 2015). Moreover, HDMBOA-Glc and HDM₂BOA-Glc accumulate upon insect herbivory and fungus infection (Oikawa et al., 2004; Glauser et al., 2011; Köhler et al., 2015), indicating that genes involved in DIMBOA-Glc metabolism are differently regulated compared with genes of the core pathway. Indeed, *Bx10*, *Bx11*, *Bx12*, *Bx13*, and *Bx14* are located on chromosomes 1 and 2 and are not part of the core pathway gene cluster. The ability to regulate these genes independently of the core pathway might allow the plant to convert DIMBOA-Glc into distinct mixtures of metabolites in response to different biotic stresses and thus would help to adapt to different ecological niches.

DIM₂BOA-Glc and HDM₂BOA-Glc Specifically Increase Plant Resistance against Aphids

Benzoxazinoid breakdown products are highly active and inhibit the growth of a variety of herbivores and pathogens (Niemeyer, 2009; Glauser et al., 2011; Ahmad et al., 2011; Meihls et al., 2013). Because of their capacity to be deglycosylated and form reactive

hemiacetals like other benzoxazinoids, we hypothesized that the 8-O-methylated compounds, DIM₂BOA-Glc and HDM₂BOA-Glc, would also decrease the performance of chewing herbivores, but expected that the changes in polarity due to the additional methoxylation may result in changes in digestive stability (Glauser et al., 2011) and herbivore growth suppression. However, our experiments with NILs differing in their BX13 activity did not confirm these hypotheses: None of the four tested chewing herbivores showed a significant change in weight gain with variation in the content of the 8-O-methylated benzoxazinoids. Our benzoxazinoid profiling experiments revealed no negative feedback effects of BX13 on other benzoxazinoids, which allows us to rule out metabolic trade-offs as an explanation for the absence of herbivore growth effects in the BX13 NILs. Many chewing herbivores seem to be able to circumvent benzoxazinoid toxicity by reglycosylating the aglucones (Sasai et al., 2009; Glauser et al., 2011; Maag et al., 2014; Wouters et al., 2014). Because of this mechanism, even the generalist Egyptian cotton leafworm is able to tolerate DIMBOA concentrations of 200 $\mu\text{g g}^{-1}$ FW (Glauser et al., 2011). It is therefore possible that the relatively low concentrations of DIM₂BOA-Glc and HDM₂BOA-Glc in *Bx13*NIL-B73 were within the range of benzoxazinoid tolerance of the different caterpillars tested.

Previous studies illustrated that benzoxazinoids can act as feeding stimulants and foraging cues for specialist maize feeders (Rostás, 2007; Robert et al., 2012; Köhler et al., 2015). The preference of the fall armyworm for young maize leaves for instance depends on the presence of benzoxazinoids (Köhler et al.,

2015). Our choice experiments demonstrate that the fall armyworm prefers to feed on DIM₂BOA-Glc and HDM₂BOA-Glc-producing plants, which suggests that these compounds stimulate the feeding of this maize pest. Feeding stimulation by plant secondary metabolites is a general phenomenon among specialized insects and may help herbivores to recognize host plants and to use plant secondary metabolites for self-defense (Erb et al., 2013; Nishida, 2014). Whether the fall armyworm derives any benefits from feeding on DIM₂BOA-Glc and HDM₂BOA-Glc-containing plants remains to be elucidated.

In contrast to chewing herbivores, we observed that the presence of DIM₂BOA-Glc and HDM₂BOA-Glc was associated with a significant reduction of aphid reproduction (Figure 8). This observation suggests that Bx13 products act as specific resistance factors in maize against aphids and possibly other phloem-feeding insects. However, although the *Bx13*-B73 and *Bx13*-Oh43 NILs vary at <0.5% of the maize genome, we cannot completely rule out the possibility that genes other than *Bx13* affect aphid reproduction on these inbred lines. Aphids seem to be more susceptible to benzoxazinoids than caterpillars, as their growth is more strongly affected by mutations in the core benzoxazinoid pathway (Ahmad et al., 2011; Köhler et al., 2015; Betsiashvili et al., 2015). It is therefore possible that small changes in benzoxazinoid patterns have more profound impacts on their physiology. Alternatively, DIM₂BOA-Glc and HDM₂BOA-Glc may have specific negative impacts on aphids. More detailed experiments would be necessary to test this hypothesis. In earlier studies, we demonstrated that DIMBOA-Glc concentrations are positively associated with callose deposition and aphid resistance and that DIMBOA induces callose deposition (Ahmad et al., 2011; Meihls et al., 2013). By contrast, our DIM₂BOA-Glc and HDM₂BOA-Glc measurements across the NAM population show no clear correlation with aphid-induced callose deposition, as measured earlier (Meihls et al., 2013). We therefore propose that direct toxicity rather than indirect effects on callose deposition are responsible for the *Bx13*-dependent increase in aphid resistance.

Conclusions

Plant defense compounds are known for their astonishing variation in structure, biosynthesis, and function. Here, we show that even for a small family of defense compounds, the benzoxazinoids with ~20 members (Niemeyer, 2009), there is unexpected variability. For two maize benzoxazinoids with an additional methoxy function at C-8, biosynthesis involves the expected enzymes (2-oxoglutarate-dependent dioxygenases and *O*-methyltransferases), but proceeds via an unprecedented route. While other benzoxazinoids have been shown to act as direct defenses to chewing herbivores and as defense signaling compounds, the 8-*O*-methylated benzoxazinoids of maize appear to target phloem-feeding herbivores.

METHODS

Plant and Insect Material

Maize (*Zea mays*) plants were grown in commercially available potting soil (Tonsubstrat; Klasmann), in a climate-controlled chamber with a 16-h photoperiod, 1 mmol (m²)⁻¹ s⁻¹ of photosynthetically active radiation, a temperature cycle of 22°C/18°C (day/night), and 65% relative humidity. Plants with three fully developed leaves were used in all experiments.

Caterpillars of Egyptian cotton leafworm (*Spodoptera littoralis*) and beet armyworm (*Spodoptera exigua*), both obtained from Syngenta, were reared on an artificial diet based on white beans (Bergomaz and Boppre, 1986) at 20 and 22°C, respectively, under natural light. Caterpillars of fall armyworm (*Spodoptera frugiperda*) were kindly provided by Ted Turlings (FARCE laboratory, University of Neuchâtel, Switzerland) and reared on an artificial diet. *Diabrotica balteata* larvae were reared as described (Robert et al., 2012). Eggs of beet armyworm (*S. exigua*) for insect growth experiments were obtained from Benzon Research and were hatched at 23°C. A maize leaf aphid (*Rhopalosiphum maidis*) colony, initially collected in New York by Stewart Gray (USDA-ARS, Ithaca, NY), was maintained on B73 seedlings in a growth chamber with a 16:8 h light:dark photoperiod at constant 23°C.

For artificial herbivory treatments, plants were scratched on the youngest leaf over 2 cm² with a razor blade and 5 μL of *S. exigua* spit was applied (*n* = 5). Damage was inflicted on one side of the midrib only to be able to distinguish local and systemic induction. Control plants remained undamaged (*n* = 5). Control leaves as well as the damaged and undamaged halves of the treated leaves were collected separately after 0, 24, 48, and 72 h.

Deglucosylation Activity

*Bx13*NIL-Oh43 and *Bx13*NIL-B73 plants were infested with six first-instar *S. frugiperda* larvae or left uninfested as controls (*n* = 4). Three days later, leaf tissue was collected, ground to a fine powder in liquid nitrogen, aliquoted into 50 mg batches, and incubated at 37°C for 1, 2, 3, or 10 min. Nonincubated samples were used as controls. After incubation, all reactions were stopped by adding 500 μL of water:methanol:FA (50:50:0.5 [v/v] methanol, LC-MS-grade, Merck; Milli-Q water, Millipore; formic acid, analytical-grade, Thermo Fischer Scientific), and BXDs were quantified as described below.

Generation of *Bx13* Near Isogenic Lines

Using a previously described approach (Mijares et al., 2013; Tuinstra et al., 1997), NILs were made from RILs of B73 and Oh43, which contain a natural *Bx13* knockout mutation (Figure 4A). B73 × Oh43 RIL genotype data (www.panzea.org) were used to identify Z022E0081, a line that was still heterozygous in the region of the *Bx13* gene polymorphism after the sixth generation of inbreeding (www.panzea.org; Supplemental Figure 7A). Line Z022E0081 was self-pollinated to produce progeny that were segregating at *Bx13* and other remaining heterozygous loci. DNA from each of the predicted regions of heterozygosity was amplified by PCR using GoTaq Polymerase (Promega), the primers listed in Supplemental Table 7, and the PCR cycle 94°C for 3 min, 34 cycles of 94°C for 30 s, 57°C for 30 s, and 72°C for 1 min, followed by 72°C extension for 10 min. Four predicted regions of heterozygosity were found to be already homozygous in our isolate of Z022E0081, which had been inbred for two generations after the original genotyping data (www.panzea.org) were generated. Among 37 tested progeny lines, a pair of NILs was identified that was (1) homozygous for either the B73 or the Oh43 allele of *Bx13* and (2) homozygous with the same genotype at other loci that had been heterozygous in Z022E0081 (Supplemental Figure 7B). The variable region containing the *Bx13* in the genotyped NIL pair is 10 cM genetic distance, corresponding to 4.7 Mb of DNA sequence and 185 predicted genes (www.maizgdb.org; RefGen v2). The two NILs were self-pollinated and progeny were used for subsequent experiments.

Extraction and Analysis of Benzoxazinoids

Plant material was ground to a fine powder under liquid nitrogen. For extraction, frozen powder was transferred to precooled 2-mL microcentrifuge tubes and weighed, and three volumes of extraction solvent methanol:water:FA (50:50:0.5 v/v; methanol, LC-MS-grade, Merck; Milli-Q water, Millipore; formic acid, analytical-grade, Thermo Fischer Scientific)

was added. The tubes were immediately mixed until the powder was completely dispersed, and two chrome steel beads (4 mm diameter) were added to each tube. Plant tissues were subsequently extracted using a paint shaker (model S0-10 M; Fluid Management), at 10 Hz for 4 min and cell debris was sedimented at 13,000g for 30 min. The supernatant was stored at -20°C before analysis.

Plant extracts from the NAM screening, induction experiments (P39 and B73), and NIL screening were analyzed using LC-MS/MS. Chromatography was performed on an Agilent 1200 HPLC system (Agilent Technologies). Separation was achieved on a Zorbax Eclipse XDB-C18 column (50×4.6 mm, $1.8 \mu\text{m}$; Agilent Technologies) with aqueous formic acid (0.05%) and methanol employed as mobile phases A and B, respectively. The following elution profile was used: 0 to 0.5 min, 90% A; 0.5 to 1 min, 90 to 79% A; 1 to 10 min, 79 to 76% A; 10 to 11 min, 76 to 50% A; 11 to 13 min, 50 to 0% A; and 13 to 16 min, 90% A. The mobile phase flow rate was 0.8 mL min^{-1} and the column temperature was maintained at 25°C . The injection volume was $5 \mu\text{L}$. The liquid chromatography was coupled to an API 3200 tandem mass spectrometer (Applied Biosystems) equipped with a Turbospray ion source operated in negative ionization mode (for detailed parameters, see Supplemental Table 8). Multiple reaction monitoring was used to monitor the parent ion > product ion transition for each analyte. Analyst 1.5 software (Applied Biosystems) was used for data acquisition and processing. Absolute concentrations of benzoxazinoids were determined using external calibration curves obtained from purified DIMBOA-Glc. For calibration, 31.3, 62.5, 125, 250, and 500 ng/mL solutions were analyzed prior to and after measurements. DIM₂BOA-Glc and HDM₂BOA were quantified using response factors of 0.9 and 8.9, respectively, compared with DIMBOA-Glc. Response factors were defined by determining the ratio of multiple reaction monitoring intensities and intensities of the optical signal at 275 nm for these compounds.

Bx13NIL-B73 and *Bx13NIL-Oh43 BXD* profiles upon tissue disruption (deglycosylation activity) were analyzed as follows: Plant extracts were analyzed by liquid chromatography-tandem UV and mass spectrometry using an Acquity UPLC I-Class system equipped with an Acquity UPLC photodiode array (PDA eX) detector and an Acquity UPLC mass detector (QDa). The chromatographic separation was achieved using a Waters Acquity UPLC BEH C18 ($2.1 \text{ mm} \times 100 \text{ mm}$, $1.7 \mu\text{m}$) at 40°C using aqueous formic acid (0.05%) and acetonitrile (Fisher Chemicals) with 0.05% formic acid as mobile phases A and B, respectively. The injection volume was $2.5 \mu\text{L}$ and the flow rate was kept constant at 0.4 mL min^{-1} . The gradient system was as follows: 0 to 9.65 min: 97 to 83.6% A; 9.65 to 11 min: 83.6-0% A; 11 to 13 min: 0 to 0% A; 13 to 13.10 min: 0 to 97% A; and 13.10 to 15 min: 97 to 97% A. UV spectra were monitored from 190 to 790 nm. The mass spectrometer was operated in negative mode to scan masses from 150 to 650 D (ESI: 0.8 V, cone voltage: 70 V) and for single ion recording in positive mode (SIR 194, ESI: 0.8 V) with a 5-Hz sampling frequency. Data were processed using MassLynx (Waters). Absolute concentrations of benzoxazinoids were calculated using external calibration curves of purified DIMBOA-Glc, HDMBOA-Glc, and MBOA (Sigma-Aldrich) at concentrations ranging from 3.125 to $50 \mu\text{g mL}^{-1}$. HDM₂BOA-Glc, DIM₂BOA-Glc, HBOA-Glc, DIBOA-Glc, and DIMBOA were quantified using response factors of 4.02, 0.85, 4.71, 1.02, and 0.36, respectively, calculated as described above. Plant extracts from the recombinant inbred lines were analyzed as described elsewhere (Glauer et al., 2011).

Benzoxazinoids in roots of the intercrossed B73 \times Mo17 population were measured as follows: Maize seedling roots frozen in liquid nitrogen were manually ground in a mortar and pestle and transferred to 2-mL microcentrifuge tubes and weighed. Three microliters of extraction solvent (30:69.9:0.1 methanol, LC-MS-grade water [Sigma-Aldrich], formic acid) were added per mg of maize tissue. The extraction solvent was spiked with 0.075 mM 2-benzoxazolinone as an internal standard. Ground tissue and extraction solvent were mixed by vortexing and incubated on a Labquake Rotisserie Shaker (Thermo Scientific) at 4°C for 40 min. Solid debris was

separated from solvent by centrifuging at 11,000g for 10 min. For each sample, 200 μL extract was filtered through a 0.45-micron filter plate by centrifuging at 200g for 3 min. LC-MS/MS analysis was performed on an Ultimate 3000 UPLC system attached to a 3000 Ultimate diode array detector and a Thermo Q Exactive mass spectrometer (Thermo Scientific). The samples were separated on a Titan C18 $7.5 \text{ cm} \times 2.1 \text{ mm} \times 1.9 \mu\text{m}$ Supelco Analytical Column (Sigma-Aldrich) at the flow rate of 0.5 mL min^{-1} , using a gradient flow of 0.1% formic acid in LC-MS-grade water (eluent A) and 0.1% formic acid in acetonitrile (eluent B) with conditions as follows: 0% B at 0 min, linear gradient to 100% B at 7 min, and linear gradient to 0% B at 11 min. Mass spectral parameters were set as follows: negative spray voltage, 3500 V; capillary temperature, 300°C ; sheath gas, 35 (arbitrary units); aux gas 10 (arbitrary units); probe heater temperature, 200°C with an HESI probe. Full-scan mass spectra were collected (R:35000 full width at half maximum, m/z 200; mass range: m/z 50 to 750) in negative mode. The quantification was done using a SIM chromatogram measured for m/z 240 using Excalibur 3.0 software. The relative DIM₂BOA content of each sample was estimated from the ratio of the DIM₂BOA peak area (mass range of m/z 240.0 to 240.2 and retention time 2.25 min) relative to 2-benzoxazolinone (mass range of m/z 134.0 to 134.2 and retention time 3.26 min), which was used as an internal standard. An annotation of benzoxazinoid derivatives by t_R and their fragmentation patterns is given in Supplemental Table 9.

Mapping Analysis

Plants from individual sets of recombinant inbred lines (B73 \times P39) were potted in 200-cm³ volume plastic pots. The soil consisted of field soil (5/10; Ricoter), peat (4/10; Ricoter), and sand (1/10; Migros Do It). Plants with three fully developed leaves were induced as described above ($n = 5$). After 48 h, the induced half of the leaf (one side of the vein, "local") and the undamaged half ("systemic part") were collected. As induction changes benzoxazinoid levels in the local part but not in the systemic part of the leaves (Supplemental Figure 1), the systemic parts were used to map constitutive benzoxazinoids, while the local parts were used to map induced levels. Seeds of 80 maize RILs from the intercrossed B73 \times Mo17 population (Lee et al., 2002) were germinated in moisturized rolls of germination paper (12 seeds per RIL per roll). Germinated seedlings were transplanted to 10×10 -cm plastic pots with Turface MVP calcined clay (Profile Products) when their primary roots reached ~ 9 cm long. Transplanted seedlings were maintained in 16:8 light: dark growth conditions at 26°C and 70% relative humidity for 6 d. Seedling roots were harvested and frozen in liquid nitrogen.

The QTL analysis was done by composite interval mapping using the Windows QTL Cartographer software version 2.5 (Wang et al., 2012). The experimental LOD threshold was determined by permutation tests with 500 repetitions at the significance level of 0.05. All analyses were performed using the default settings in the WinQTL program as follows: the CIM program module = Model 6: Standard Model, walking speed = 2 cM, control marker numbers = 5, window size = 10 cM, regression method = backward regression method. Maize genetic marker data were downloaded from www.panzea.org and were used for linkage mapping using multiple sets of recombinant lines from the NAM population. A list of all RILs used for mapping in this study is given in Supplemental Table 10.

Preparation of RNA and cDNA

Frozen plant material was ground to a fine powder in a liquid nitrogen precooled mortar and RNA was extracted using the RNeasy Plant Mini Kit (Qiagen) according to the manufacturer's instructions. Nucleic acid concentration, purity, and quality were assessed using a spectrophotometer (NanoDrop 2000c; Thermo Scientific) and Agilent 2100 Bioanalyzer (Agilent Technologies). Prior to cDNA synthesis, 0.75 μg RNA was treated with 1 unit of DNase (Fermentas). Single-stranded cDNA was prepared from the

DNase-treated RNA using SuperScript III reverse transcriptase and oligo(dT₂₀) primers (Invitrogen).

Gene Synthesis

The complete open reading frames of *Bx6*-Cl31A (AF540907) and *Bx7*-Cl31A (NM_001127247) were synthesized after codon optimization for heterologous expression in *Escherichia coli* by Eurofins MWG Operon (for optimized sequences, see Supplemental Figure 14). Synthetic genes were subcloned into the vector pUC57 and fully sequenced.

Cloning and Heterologous Expression

The complete open reading frames of *Bx10*-B73, *Bx11*-B73, *Bx12*-CML322, *Bx13*-P39, *Bx14*-B73, *Zrp4*-P39, AC209819.3_FG005, GRMZM2G100754, GRMZM2G097297, GRMZM2G023152, GRMZM2G102863, and GRMZM2G141026 were amplified from cDNA with the primer pairs listed in Supplemental Table 5. *Bx6*-Cl31A, *Bx7*-Cl31A, GRMZM2G093092, and GRMZM2G106172 were amplified from plasmids containing the respective synthesized codon-optimized open reading frames as described above. The obtained PCR products were cloned as blunt fragments into the sequencing vector pCR-Blunt II-TOPO (Invitrogen) and both strands were fully sequenced. For heterologous expression with an N-terminal His-Tag, the genes were inserted into the expression vector pET100/D-TOPO (Invitrogen). The OMT genes *Bx10*-B73, *Bx11*-B73, *Bx12*-CML322, *Bx14*-B73, *Zrp4*-P39, AC209819.3_FG005, GRMZM2G100754, GRMZM2G097297, GRMZM2G023152, GRMZM2G102863, GRMZM2G141026, GRMZM2G106172, and GRMZM2G093092 were expressed in the *E. coli* strain BL21(DE3) (Invitrogen). For expression, liquid cultures of bacteria harboring the expression construct were grown at 37°C to an OD₆₀₀ of 0.6 to 0.8. IPTG was added to a final concentration of 1 mM, and the cultures were incubated for 20 h at 18°C and 200 rpm. The two 2ODD genes *Bx6*-Cl31A and *Bx13*-P39 were introduced in the *E. coli* strain C41(DE3) pLysS (Lucigen), and heterologous expression was performed as described by Jaganaman et al. (2007). The cells were sedimented for 5 min at 5000g and 4°C. For breaking-up the cells, the pellet was resuspended in ice-cold 4 mL 50 mM Tris-HCl (pH 8.0) containing 0.5 M NaCl, 20 mM imidazole, 50 mM 2-mercaptoethanol, and 10% glycerol and subsequently subjected to ultrasonication (4 × 20 s; Bandelin UW2070). The debris was separated by centrifugation for 20 min at 16,100g and 4°C. N-terminal His-tagged proteins were purified using Ni-NTA spin columns (Qiagen) according to the manufacturer's instructions. The purified proteins were eluted with 50 mM Tris-HCl (pH 8.0) containing 0.5 M NaCl, 250 mM imidazole, and 10% glycerol. Eluates of the dioxygenases BX6 and BX13 were directly used for enzyme assays. For purified OMT, the salt was removed by gel filtration using Illustra™ NAPTM-10 columns (GE Healthcare) and the proteins were redissolved in 50 mM Tris-HCl (pH 7.0) containing 50% glycerol.

In Vitro Characterization of Recombinant Enzymes

2ODD and OMT activities were tested using enzyme assays containing purified recombinant protein, benzoxazinoid substrates, and the respective cosubstrates. 2ODD assays with recombinant BX6 or BX13 were performed with 5 mM 2-mercaptoethanol, 5 mM 2-oxoglutarate, 0.5 mM ascorbate, 0.25 mM ferric chloride, 0.2 mg mL⁻¹ substrate (DIMBOA-Glc or HDMBOA-Glc), and 0.5 μg desalted enzyme dissolved in 100 mM Tris-HCl, pH 7.0, in a total volume of 100 μL. OMT assays were performed with 0.2 mM DTT, 0.2 mM EDTA, 0.5 mM S-adenosyl-L-methionine, 0.2 mg mL⁻¹ substrate, and 0.5 μg desalted enzyme solved in 100 mM Tris-HCl, pH 7.5, in a volume of 100 μL. For BX7 activity assays, TRIMBOA-Glc, which was purified as described below from 300 pooled BX13 enzyme assays, was used as substrate. BX14 activity was tested with DIMBOA-Glc, DIM₂BOA-Glc, and TRIMBOA-Glc. All assays were incubated in glass vials overnight

at 25°C at 350 rpm using a ThermoMixer comfort 5355 (Eppendorf). The reaction was stopped with 5 μL formic acid, 99% pure (Sigma-Aldrich) and centrifuged for 15 min at 13,000g. Product formation was monitored by the analytical methods described above. Metabolite identities were confirmed using authentic standard compounds.

Semi-Preparative Purification of DIMBOA-Glc and TRIMBOA-Glc

Supernatants of terminated BX13 assays were pooled (total volume of 30 mL) and chromatographically separated using an Agilent 1100 HPLC system (Agilent Technologies). The separation was achieved on a Nucleodur Sphinx RP column (250 × 4.6 mm, 5 μm; Macherey Nagel) with aqueous formic acid (0.1%) and acetonitrile (LC-MS grade; VWR Chemicals) employed as mobile phases A and B, respectively, with the following elution profile: 0 to 10 min, 10–70% B in A; 10 to 11 min 100% B; 11 to 14 min 10% B. The mobile phase flow rate was 1.1 mL min⁻¹ and the column temperature was maintained at 25°C. A volume of 100 μL was injected. Benzoxazinoids were traced at the absorption maximum of 270 nm and fractions between 9.2 to 9.4 and 10.6 to 11.4 min were collected with a SF-2120 Super Fraction collector (Advantec). Both fractions were concentrated with a Rotavapor R-114 rotary evaporation system (Büchi) and washed twice with aqueous methanol and subsequently verified by LC-MS/MS (see Extraction and Analysis of Benzoxazinoids). Collected and purified fractions containing 100 μg of the enzymatic product TRIMBOA-Glc and 700 μg DIMBOA-Glc, respectively, were dissolved in 50 μL Milli-Q water and freeze-dried for NMR analysis.

Nuclear Magnetic Resonance Spectroscopy

¹H NMR, ¹H, ¹H COSY, HMBC, and HSQC spectra were measured at 300K on a Bruker Avance III HD 700 NMR spectrometer (Bruker Biospin) using a cryogenically cooled 1.7-mm TCI ¹H(¹³C) probe. The operating frequency was 700.45 MHz for ¹H and 176.13 MHz for ¹³C. MeOH-*d*₄ was used as a solvent and tetramethylsilane as an internal standard. The residual HDO signal in the ¹H NMR spectra was suppressed using the NOESY solvent-presaturation (noesypr1d) pulse program.

Identification of TRIMBOA-Glc

The ¹H NMR spectrum of TRIMBOA-Glc displayed doublets of an AX spin system assignable to the aromatic protons H-5 (δ 6.96) and H-6 (δ 6.63) (*J*_{H5-H6} = 8.9 Hz), a singlet (1H) at a low field (δ 5.96) attributable to H-2 at the hydroxylated carbon atom of the 1,4-oxazin-3-one ring, and a singlet (integrating for three protons) with a chemical shift (δ 3.90) characteristic of a methoxy group on the aromatic ring. In addition, a complete set of ¹H NMR signals of the glucose unit was detected (Supplemental Table 4). The signal of H-1' (δ 4.71) shows a spin-spin coupling *J*_{H1'-H2} = 7.9 Hz characteristic of the β-configuration at the anomeric center of the glucose unit. The signal-to-noise ratio of this signal was reduced due to its proximity to the suppressed residual water signal. Attachment of the glucose to C-2 of the benzoxazinoid moiety was established by means of HMBC correlations of H-1' with C-2 (δ 98.1) and H-2 with C-1' (δ 104.3). The signal of H-2 also shows cross signals with C-3 (δ 157.1) and C-9 (δ 136.3), supporting its assignment to this particular proton. HMBC correlations of H-5 and H-6 (Figure 3C) and the corresponding ¹³C chemical shifts proved that the carbon atoms C-7 (δ 148.9) and C-8 (δ 138.1) in the aromatic ring were oxygenated. The question whether the oxygen functionality at C-7 or C-8 carries the O-methyl group was established by means of the correlation between the O-methyl signal and C-8 observed in the HMBC spectrum (Figure 3C). Thus, the structure of TRIMBOA-Glc was identified as 2-(2,4,7-trihydroxy-8-methoxy-1,4-benzoxazin-3-one)-β-D-glucopyranose. Further HMBC cross signals, together with HSQC correlations, completed the assignment of the chemical shifts of the remaining carbon atoms (Supplemental Table 4).

Sequence Analysis and Tree Reconstruction

Multiple sequence alignments of maize *OMT* and *2ODD* genes similar to *Bx7* and *Bx6*, respectively, were computed using the GUIDANCE2 server (<http://guidance.tau.ac.il/ver2/>) and the MAFFT (codon) multiple sequence alignment algorithm (Supplemental Data Sets 1 and 2). Based on the MAFFT alignments, trees were reconstructed with MEGA5 (Tamura et al., 2011) using a maximum likelihood algorithm (general time-reversible model, gamma distributed rates among sites). Codon positions included were 1st+2nd+3rd+noncoding. All positions with <90% site coverage were eliminated. Ambiguous bases were allowed at any position. A bootstrap resampling analysis with 1000 replicates was performed to evaluate the topology of the generated trees.

qRT-PCR Analysis

Relative quantification of *Bx7*, *Bx13*, and *Bx14* gene expression was performed using qRT-PCR with the qPCR system MxPro Mx300P (Stratagene). For the amplification of gene fragments with a length of 150 to 250 bp, specific primer pairs were designed having a melting temperature equal to or higher than 60°C, a GC content of between 35 and 55%, and a primer length in the range of 20 to 25 nucleotides (Supplemental Table 7). Primer specificity was confirmed by agarose gel electrophoresis, melting point curve analysis, and sequence verification of cloned PCR amplicons. Primer pair efficiency was determined using the standard curve method with fivefold serial dilution of cDNA and was found to be between 90 and 105%. As reference, the actin gene *Zm-Actin1* (accession number MZEA1G) was used. cDNA was prepared as described above, and 1 μ L cDNA was used in 20- μ L reactions containing Brilliant III SYBR Green qPCR Master Mix (Stratagene) and ROX as the reference dye. Biological replicates were analyzed as triplicates. The PCR consisted of an initial incubation at 95°C for 3 min followed by 50 amplification cycles with 20 s at 95°C and 20 s at 60°C. For each cycle, reads were taken during the annealing and the extension step. At the end of cycling, the melting curves were gathered for 55 to 95°C. Data for the relative quantity of calibrator average (dRn) were exported from MxPro software.

Discovery of Natural *Bx13* Knockout Variants in HapMap3 Maize Lines

To discover naturally occurring knockout variants of *Bx13*, sensitive remapping of Illumina reads from 916 diverse maize lines in HapMap 3.1 was performed (Bukowski et al., 2015). Paired-end reads from each sample, previously aligned using BWA-MEM (Bukowski et al., 2015), were isolated from the existing BAM files within 10 kb of AC148152.3_FGT005 (*Bx13*; AGPv3 Chr2:231942642-231964277). These were then realigned to the same *Bx13*-proximal region of AGPv3 using Stampy (v. 1.0.23) with default options (Lunter and Goodson, 2011). Following alignment, Platypus was used to call variants, with option “assemble=1” (Rimmer et al., 2014). SNPeff was then used to infer the probable biochemical consequences of the variants (Cingolani et al., 2012). Samples containing putative frameshifts or start codon losses were candidates for knockout mutations. These mutations were confirmed by DNA sequencing.

Insect Bioassays

To test caterpillar preference, *S. frugiperda* larvae were given the choice between one *Bx13*NIL-Oh43 and one *Bx13*NIL-B73 plant sown together in 11-cm-high, 4-cm-diameter plastic pots ($n = 30$). All plants were infested with three first instar *S. frugiperda* larvae. To prevent larvae from escaping, each pot was surrounded by a transparent plastic film (PPC-12.10A; Kodak). After 2 d, plant damage was recorded every day for 10 d. After 4 d, the number of larvae feeding on each plant was recorded every 12 h for 6 d.

To measure *S. frugiperda* weight gain, individual *Bx13*NIL-Oh43 and *Bx13*NIL-B73 plants were infested with six first-instar *S. frugiperda* larvae

($n = 18$). To prevent larvae from escaping, all plants were covered with 1.5 liters polyethylene terephthalate bottles as described (Erb et al., 2011). Five, seven, and nine days after infestation, larval mass was determined using a microbalance (Ohaus N30330). *S. littoralis* performance was measured similarly to *S. frugiperda* performance 9 d after infestation as described above ($n = 7$ to 9). *D. balteata* performance was determined by placing six preweighed second instar *D. balteata* larvae in 5-cm-deep holes in the soil. After 6 d, all larvae were collected and weighed to determine average weight gain ($n = 8$).

For *S. exigua* growth assays, NILs containing either the Oh43 or the B73 allele at *Bx13* were planted at a depth of 1.5 cm in 200-cm³ plastic pots filled with moistened maize mix (produced by combining 0.16 m³ Metro-Mix 360 [Scotts], 0.45 kg finely ground lime, 0.45 kg Peters Unimix [Scotts], 68 kg Turface MVP [Profile Products], 23 kg coarse quartz sand, and 0.018 m³ pasteurized field soil). Plants were grown in a growth chamber (Conviron) under a 16:8-h light:dark photoperiod and 180 mmol photons/m²/s light intensity at constant 23°C and 60% relative humidity. Neonate larvae were confined on individual maize plants with perforated polypropylene bags (15 cm \times 61 cm). After 10 d, *S. exigua* larvae were harvested, lyophilized, and weighed ($n = 38$ to 52).

For measurements of aphid reproduction, 10 adult *R. maidis* from B73 plants were confined on 2-week-old *Bx13*NIL-Oh43 and *Bx13*NIL-B73 plants (grown as described above for *S. exigua* experiments) using perforated polypropylene bags. Experimental plants with aphids were placed in the same growth room as the aphid colony. Seven days after infestation, the remaining adults and progeny were counted. As it was not possible to determine whether missing adult aphids had died, absconded, or were otherwise not found, aphid fecundity was calculated as progeny per adult aphid remaining at the end of the experiment. This experiment was independently replicated twice with comparable results.

Statistical Analysis

Statistical significance was tested using analysis of variance in SigmaPlot 11.0 for Windows (Systat Software). Whenever necessary, the data were \ln transformed to meet statistical assumptions, such as normality and homogeneity of variances.

Accession Numbers

Sequence data from this article can be found in GenBank/EMBL data libraries under the following accession numbers: *Bx6*, AY104457; *Bx7*-Cl31A, NM_001127247; *Bx10*-B73, AGS16666; *Bx11*-B73, AGS16667; *Bx12*-CML322, AGS16668; *Bx13*-P39, KU521787, *Bx13*-Oh43, KU521786; *Bx14*-B73, KU521788; *Bx14*-Il14H, KU521789; *OMT1*-B73, ABQ58826; and *Zrp4*, NM_001112219.

Supplemental Data

Supplemental Figure 1. Herbivory-induced changes in HDM₂BOA-Glc and DIM₂BOA-Glc are restricted to the wound site.

Supplemental Figure 2. LC-MS/MS fragmentation patterns of DIMBOA-Glc and TRIMBOA-Glc.

Supplemental Figure 3. Substrate specificity of the 2-oxoglutarate-dependent dioxygenases BX6 and BX13.

Supplemental Figure 4. Nucleic acid alignment of *Bx13*-P39 and *Bx13*-Oh43.

Supplemental Figure 5. Amino acid alignment of 2-oxoglutarate-dependent dioxygenases.

Supplemental Figure 6. Some *Bx13* alleles contain a mutated start codon.

Supplemental Figure 7. Generation of *Bx13* near isogenic lines for the *Bx13* locus on chromosome 2.

Supplemental Figure 8. Enzymatic activity of O-methyltransferases similar to Bx7 toward TRIMBOA-Glc.

Supplemental Figure 9. Enzymatic activity of O-methyltransferases similar to Bx7 toward DIMBOA-Glc and DIM₂BOA-Glc.

Supplemental Figure 10. Nucleic acid alignment of Bx14-B73 and Bx14-II14H.

Supplemental Figure 11. In vitro activity of Bx14-II14H and the presence/absence of a 30-bp in-frame insertion in Bx14 within the NAM population.

Supplemental Figure 12. Effect of BX13 on benzoxazinoid accumulation and hydrolysis.

Supplemental Figure 13. BX13 decreases aphid performance (2nd independent experiment).

Supplemental Figure 14. Codon-optimized gene sequences of Bx6-CI31A, Bx7-CI31A, GRMZM2G093092, and GRMZM2G106172 synthesized for expression in *Escherichia coli*.

Supplemental Table 1. Concentrations of DIM₂BOA-Glc in undamaged controls and *Spodoptera exigua*-treated maize leaf samples.

Supplemental Table 2. Concentrations of HDM₂BOA-Glc in undamaged controls and *Spodoptera exigua*-treated maize leaf samples.

Supplemental Table 3. Estimates of the additive allelic effect under the hypotheses H1, with the additive allelic effect, a, distinguishable from zero and the dominance deviation equal to zero.

Supplemental Table 4. ¹H- and ¹³C NMR data of TRIMBOA-Glc (700.45 MHz for ¹H and 176.13 MHz for ¹³C, MeOH-*d*₄).

Supplemental Table 5. Primers for open reading frame amplification of investigated genes.

Supplemental Table 6. P values of two-way repeated-measured ANOVA to test for genotype and time:genotype interaction (time*genotype) effects in the Bx13 NILs in the experiment shown in Supplemental Figure 12.

Supplemental Table 7. qRT-PCR primers used to determine expression levels of Bx7, Bx13, and Bx14 and primers for the detection of SNP markers.

Supplemental Table 8. LC-MS/MS settings used for the analysis of benzoxazinoids.

Supplemental Table 9. Annotation of benzoxazinoid derivatives by *t_R* and their fragmentation patterns.

Supplemental Table 10. List of RILs used for mapping in this study.

Supplemental Data Set 1. FASTA file of the alignment of maize 2ODD genes similar to Bx6-B73.

Supplemental Data Set 2. FASTA file of the alignment of maize OMT genes similar to Bx7.

ACKNOWLEDGMENTS

We thank Tamara Krügel and all the MPI-CE gardeners as well as Christopher Ball and all the IPS gardeners for their support in growing the maize plants. We thank Grit Kunert for her help with the statistics, Stefanie Schirmer, Oliver Dosh, and Julian Riederer for their contribution to the experiments, and Meena Haribal for assistance with HPLC-MS analysis. The research was funded by two Sinergia Grants of the Swiss National Science Foundation (136184 and 160786), an ERA-CAPS project (BENZEX), the Max Planck Society, U.S. National Science Foundation Awards 1358843, 1339237, and 1139329 to G.J. and 1238014 to E.S.B., and the U.S.

Department of Agriculture. Research activities by C.A.M.R. were supported by the Swiss National Science Foundation (PBNEP3_140196).

AUTHOR CONTRIBUTIONS

V.H., C.A.M.R., E.S.B., J.G., G.J., M.E., and T.G.K. designed the research. V.H., C.A.M.R., R.A.R.M., M.E., E.R.-M., G.J., and J.N.C. carried out the experimental work. V.H., C.A.M.R., R.A.R.M., W.B., E.R.-M., G.J., B.S., and M.E. analyzed data. E.S.B. contributed essential research materials. V.H., C.A.M.R., G.J., M.E., and T.G.K. wrote the article. All authors read and approved the final manuscript. V.H. and C.A.M.R. contributed equally to the study and share first authorship. G.J., M.E., and T.G.K. contributed equally to the study and share senior authorship.

Received February 2, 2016; revised June 3, 2016; accepted June 14, 2016; published June 17, 2016.

REFERENCES

- Ahmad, S., Veyrat, N., Gordon-Weeks, R., Zhang, Y., Martin, J., Smart, L., Glauser, G., Erb, M., Flors, V., Frey, M., and Ton, J. (2011). Benzoxazinoid metabolites regulate innate immunity against aphids and fungi in maize. *Plant Physiol.* **157**: 317–327.
- Babcock, G.D., and Esen, A. (1994). Substrate specificity of maize β -glucosidase. *Plant Sci.* **101**: 31–39.
- Bergomaz, R., and Boppre, M. (1986). A simple instant diet for rearing arctiids and other moths. *J. Lepidopt. Soc.* **40**: 131–137.
- Berim, A., Kim, M.-J., and Gang, D.R. (2015). Identification of a unique 2-oxoglutarate-dependent flavone 7-O-demethylase completes the elucidation of the lipophilic flavone network in basil. *Plant Cell Physiol.* **56**: 126–136.
- Betsiashvili, M., Ahern, K.R., and Jander, G. (2015). Additive effects of two quantitative trait loci that confer *Rhopalosiphum maidis* (corn leaf aphid) resistance in maize inbred line Mo17. *J. Exp. Bot.* **66**: 571–578.
- Bukowski, R., et al. (2015). Construction of the third generation *Zea mays* haplotype map. *bioRxiv* 10.1101/026963.
- Cambier, V., Hance, T., and de Hoffmann, E. (1999). Non-injured maize contains several 1,4-benzoxazin-3-one related compounds but only as glucoconjugates. *Phytochem. Anal.* **10**: 119–126.
- Cambier, V., Hance, T., and de Hoffmann, E. (2000). Variation of DIMBOA and related compounds content in relation to the age and plant organ in maize. *Phytochemistry* **53**: 223–229.
- Cingolani, P., Platts, A., Wang, L., Coon, M., Nguyen, T., Wang, L., Land, S.J., Lu, X., and Ruden, D.M. (2012). A program for annotating and predicting the effects of single nucleotide polymorphisms, SnpEff: SNPs in the genome of *Drosophila melanogaster* strain w1118; iso-2; iso-3. *Fly (Austin)* **6**: 80–92.
- Czjzek, M., Cicek, M., Zamboni, V., Bevan, D.R., Henrissat, B., and Esen, A. (2000). The mechanism of substrate (aglycone) specificity in beta -glucosidases is revealed by crystal structures of mutant maize beta -glucosidase-DIMBOA, -DIMBOAGlc, and -dhurrin complexes. *Proc. Natl. Acad. Sci. USA* **97**: 13555–13560.
- Dafoe, N.J., Huffaker, A., Vaughan, M.M., Duehl, A.J., Teal, P.E., and Schmelz, E.A. (2011). Rapidly induced chemical defenses in maize stems and their effects on short-term growth of *Ostrinia nubilalis*. *J. Chem. Ecol.* **37**: 984–991.
- Erb, M., Balmer, D., De Lange, E.S., Von Meroy, G., Planchamp, C., Robert, C.A.M., Röder, G., Sobhy, I., Zwahlen, C., Mauch-Mani, B., and Turlings, T.C.J. (2011). Synergies and trade-offs between insect and pathogen resistance in maize leaves and roots. *Plant Cell Environ.* **34**: 1088–1103.

- Erb, M., Flors, V., Karlen, D., de Lange, E., Planchamp, C., D'Alessandro, M., Turlings, T.C.J., and Ton, J. (2009). Signal signature of aboveground-induced resistance upon belowground herbivory in maize. *Plant J.* **59**: 292–302.
- Erb, M., Huber, M., Robert, C., Ferrieri, A., Machado, R.A.R., and Arce, C. (2013). The role of plant primary and secondary metabolites in root herbivore behavior, nutrition and physiology. In *Advances in Insect Physiology*, P. Evans and V. Wigglesworth, eds (Burlington, MA: Elsevier), pp. 53–95.
- Flint-Garcia, S.A., Thuillet, A.-C., Yu, J., Pressoir, G., Romero, S.M., Mitchell, S.E., Doebley, J., Kresovich, S., Goodman, M.M., and Buckler, E.S. (2005). Maize association population: a high-resolution platform for quantitative trait locus dissection. *Plant J.* **44**: 1054–1064.
- Frey, M., Chomet, P., Glawischning, E., Stettner, C., Grün, S., Winklmaier, A., Eisenreich, W., Bacher, A., Meeley, R.B., Briggs, S.P., Simcox, K., and Gierl, A. (1997). Analysis of a chemical plant defense mechanism in grasses. *Science* **277**: 696–699.
- Frey, M., Schullehner, K., Dick, R., Fiesselmann, A., and Gierl, A. (2009). Benzoxazinoid biosynthesis, a model for evolution of secondary metabolic pathways in plants. *Phytochemistry* **70**: 1645–1651.
- Ganal, M.W., et al. (2011). A large maize (*Zea mays* L.) SNP genotyping array: development and germplasm genotyping, and genetic mapping to compare with the B73 reference genome. *PLoS One* **6**: e28334.
- Gierl, A., and Frey, M. (2001). Evolution of benzoxazinone biosynthesis and indole production in maize. *Planta* **213**: 493–498.
- Glauser, G., Marti, G., Villard, N., Doyen, G.A., Wolfender, J.-L., Turlings, T.C.J., and Erb, M. (2011). Induction and detoxification of maize 1,4-benzoxazin-3-ones by insect herbivores. *Plant J.* **68**: 901–911.
- Goodwin, T.W., and Mercer, E.I. (1983). *Introduction to Plant Biochemistry*. (Oxford, UK: Pergamon Press).
- Hagel, J.M., and Facchini, P.J. (2010). Dioxygenases catalyze the O-demethylation steps of morphine biosynthesis in opium poppy. *Nat. Chem. Biol.* **6**: 273–275.
- He, P., and Moran, G.R. (2009). We two alone will sing: the two-substrate alpha-keto acid-dependent oxygenases. *Curr. Opin. Chem. Biol.* **13**: 443–450.
- Ibrahim, R.K. (1997). Plant O-methyltransferase signatures. *Trends Plant Sci.* **2**: 249–250.
- Jaganaman, S., Pinto, A., Tarasev, M., and Ballou, D.P. (2007). High levels of expression of the iron-sulfur proteins phthalate dioxygenase and phthalate dioxygenase reductase in *Escherichia coli*. *Protein Expr. Purif.* **52**: 273–279.
- Jonczyk, R., Schmidt, H., Osterrieder, A., Fiesselmann, A., Schullehner, K., Haslbeck, M., Sicker, D., Hofmann, D., Yalpani, N., Simmons, C., Frey, M., and Gierl, A. (2008). Elucidation of the final reactions of DIMBOA-glucoside biosynthesis in maize: characterization of Bx6 and Bx7. *Plant Physiol.* **146**: 1053–1063.
- Kawai, Y., Ono, E., and Mizutani, M. (2014). Evolution and diversity of the 2-oxoglutarate-dependent dioxygenase superfamily in plants. *Plant J.* **78**: 328–343.
- Köhler, A., Maag, D., Veyrat, N., Glauser, G., Wolfender, J.-L., Turlings, T.C.J., and Erb, M. (2015). Within-plant distribution of 1,4-benzoxazin-3-ones contributes to herbivore niche differentiation in maize. *Plant Cell Environ.* **38**: 1081–1093.
- Lee, M., Sharopova, N., Beavis, W.D.G.D., Grant, D., Katt, M., Blair, D., and Hallauer, A. (2002). Expanding the genetic map of maize with the intermated B73 x Mo17 (IBM) population. *Plant Mol. Biol.* **48**: 453–461.
- Lunter, G., and Goodson, M. (2011) Stampy: a statistical algorithm for sensitive and fast mapping of Illumina sequence reads. *Genome Res.* **21**: 936–939.
- Maag, D., Dalvit, C., Thevenet, D., Köhler, A., Wouters, F.C., Vassão, D.G., Gershenzon, J., Wolfender, J.L., Turlings, T.C.J., Erb, M., and Glauser, G. (2014). 3- β -D-Glucopyranosyl-6-methoxy-2-benzoxazinolone (MBOA-N-Glc) is an insect detoxification product of maize 1,4-benzoxazin-3-ones. *Phytochemistry* **102**: 97–105.
- Maresh, J., Zhang, J., and Lynn, D.G. (2006). The innate immunity of maize and the dynamic chemical strategies regulating two-component signal transduction in *Agrobacterium tumefaciens*. *ACS Chem. Biol.* **1**: 165–175.
- Marti, G., Erb, M., Boccard, J., Glauser, G., Doyen, G.R., Villard, N., Robert, C.A.M., Turlings, T.C.J., Rudaz, S., and Wolfender, J.-L. (2013). Metabolomics reveals herbivore-induced metabolites of resistance and susceptibility in maize leaves and roots. *Plant Cell Environ.* **36**: 621–639.
- McMullen, M.D., et al. (2009). Genetic properties of the maize nested association mapping population. *Science* **325**: 737–740.
- Meihls, L.N., Handrick, V., Glauser, G., Barbier, H., Kaur, H., Haribal, M.M., Lipka, A.E., Gershenzon, J., Buckler, E.S., Erb, M., Köllner, T.G., and Jander, G. (2013). Natural variation in maize aphid resistance is associated with 2,4-dihydroxy-7-methoxy-1,4-benzoxazin-3-one glucoside methyltransferase activity. *Plant Cell* **25**: 2341–2355.
- Mijares, V., Meihls, L.N., Jander, G., and Tzin, V. (2013). Near-isogenic lines for measuring phenotypic effects of DIMBOA-Glc methyltransferase activity in maize. *Plant Signal. Behav.* **8**: 4161–, 26779.
- Niemeyer, H.M. (2009). Hydroxamic acids derived from 2-hydroxy-2H-1,4-benzoxazin-3(4H)-one: key defense chemicals of cereals. *J. Agric. Food Chem.* **57**: 1677–1696.
- Nishida, R. (2014). Chemical ecology of insect-plant interactions: ecological significance of plant secondary metabolites. *Biosci. Biotechnol. Biochem.* **78**: 1–13.
- Oikawa, A., Ishihara, A., Tanaka, C., Mori, N., Tsuda, M., and Iwamura, H. (2004). Accumulation of HDMBOA-Glc is induced by biotic stresses prior to the release of MBOA in maize leaves. *Phytochemistry* **65**: 2995–3001.
- Osborn, A. (2010). Gene clusters for secondary metabolic pathways: an emerging theme in plant biology. *Plant Physiol.* **154**: 531–535.
- Raspail, C., Graindorge, M., Moreau, Y., Crouzy, S., Lefebvre, B., Robin, A.Y., Dumas, R., and Matringe, M. (2011). 4-hydroxyphenylpyruvate dioxygenase catalysis: identification of catalytic residues and production of a hydroxylated intermediate shared with a structurally unrelated enzyme. *J. Biol. Chem.* **286**: 26061–26070.
- Rimmer, A., Phan, H., Mathieson, I., Iqbal, Z., Twigg, S.R.F., Wilkie, A.O.M., McVean, G., and Lunter, G.; WGS500 Consortium (2014). Integrating mapping-, assembly- and haplotype-based approaches for calling variants in clinical sequencing applications. *Nat. Genet.* **46**: 912–918.
- Robert, C.A.M., et al. (2012). A specialist root herbivore exploits defensive metabolites to locate nutritious tissues. *Ecol. Lett.* **15**: 55–64.
- Rostás, M. (2007). The effects of 2,4-dihydroxy-7-methoxy-1,4-benzoxazin-3-one on two species of *Spodoptera* and the growth of *Setosphaeria turcica* in vitro. *J. Pest Sci.* **80**: 35–41.
- Sasai, H., Ishida, M., Murakami, K., Tadokoro, N., Ishihara, A., Nishida, R., and Mori, N. (2009). Species-specific glucosylation of DIMBOA in larvae of the rice armyworm. *Biosci. Biotechnol. Biochem.* **73**: 1333–1338.
- Schnable, P.S., et al. (2009). The B73 maize genome: complexity, diversity, and dynamics. *Science* **326**: 1112–1115.
- Schofield, C.J., and Zhang, Z. (1999). Structural and mechanistic studies on 2-oxoglutarate-dependent oxygenases and related enzymes. *Curr. Opin. Struct. Biol.* **9**: 722–731.
- Tamura, K., Peterson, D., Peterson, N., Stecher, G., Nei, M., and Kumar, S. (2011). MEGA5: molecular evolutionary genetics analysis

- using maximum likelihood, evolutionary distance, and maximum parsimony methods. *Mol. Biol. Evol.* **28**: 2731–2739.
- Tuinstra, M.R., Ejeta, G., and Goldsbrough, P.B.** (1997). Heterogeneous inbred family (HIF) analysis: A method for developing near-isogenic lines that differ at quantitative trait loci. *Theor. Appl. Genet.* **95**: 1005–1011.
- Tzin, V., Lindsay, P.L., Christensen, S.A., Meihls, L.N., Blue, L.B., and Jander, G.** (2015). Genetic mapping shows intraspecific variation and transgressive segregation for caterpillar-induced aphid resistance in maize. *Mol. Ecol.* **24**: 5739–5750.
- von Rad, U., Hüttl, R., Lottspeich, F., Gierl, A., and Frey, M.** (2001). Two glucosyltransferases are involved in detoxification of benzoxazinoids in maize. *Plant J.* **28**: 633–642.
- Wang, S.M., Basten, C.J., and Zeng, Z.B.** (2012). Windows QTL Cartographer 2.5. (Raleigh, NC: North Carolina State University).
- Wei, F., et al.** (2009). The physical and genetic framework of the maize B73 genome. *PLoS Genet.* **5**: e1000715.
- Wouters, F.C., Reichelt, M., Glauser, G., Bauer, E., Erb, M., Gershenzon, J., and Vassão, D.G.** (2014). Reglucosylation of the benzoxazinoid DIMBOA with inversion of stereochemical configuration is a detoxification strategy in lepidopteran herbivores. *Angew. Chem. Int. Ed. Engl.* **53**: 11320–11324.
- Yu, J., Holland, J.B., McMullen, M.D., and Buckler, E.S.** (2008). Genetic design and statistical power of nested association mapping in maize. *Genetics* **178**: 539–551.
- Zhou, J.-M., Fukushi, Y., Wollenweber, E., and Ibrahim, R.K.** (2008). Characterization of two *O*-methyltransferase-like genes in barley and maize. *Pharm. Biol.* **46**: 26–34.
- Zhou, S., et al.** (2009). A single molecule scaffold for the maize genome. *PLoS Genet.* **5**: e1000711.
- Zubieta, C., He, X.Z., Dixon, R.A., and Noel, J.P.** (2001). Structures of two natural product methyltransferases reveal the basis for substrate specificity in plant *O*-methyltransferases. *Nat. Struct. Biol.* **8**: 271–279.

Biosynthesis of 8-O-Methylated Benzoxazinoid Defense Compounds in Maize

Vinzenz Handrick, Christelle A.M. Robert, Kevin R. Ahern, Shaoqun Zhou, Ricardo A.R. Machado, Daniel Maag, Gaetan Glauser, Felix E. Fernandez-Penny, Jima N. Chandran, Eli Rodgers-Melnik, Bernd Schneider, Edward S. Buckler, Wilhelm Boland, Jonathan Gershenzon, Georg Jander, Matthias Erb and Tobias G. Köllner

Plant Cell 2016;28;1682-1700; originally published online June 17, 2016;
DOI 10.1105/tpc.16.00065

This information is current as of January 9, 2019

Supplemental Data	/content/suppl/2016/06/17/tpc.16.00065.DC1.html
References	This article cites 52 articles, 11 of which can be accessed free at: /content/28/7/1682.full.html#ref-list-1
Permissions	https://www.copyright.com/ccc/openurl.do?sid=pd_hw1532298X&iissn=1532298X&WT.mc_id=pd_hw1532298X
eTOCs	Sign up for eTOCs at: http://www.plantcell.org/cgi/alerts/ctmain
CiteTrack Alerts	Sign up for CiteTrack Alerts at: http://www.plantcell.org/cgi/alerts/ctmain
Subscription Information	Subscription Information for <i>The Plant Cell</i> and <i>Plant Physiology</i> is available at: http://www.aspb.org/publications/subscriptions.cfm